

Copyright © 1990, by the author(s).
All rights reserved.

Permission to make digital or hard copies of all or part of this work for personal or classroom use is granted without fee provided that copies are not made or distributed for profit or commercial advantage and that copies bear this notice and the full citation on the first page. To copy otherwise, to republish, to post on servers or to redistribute to lists, requires prior specific permission.

**BIFURCATION AND CHAOS IN
POWER SYSTEMS: A SURVEY**

by

Pravin Varaiya, Felix Wu,
and Hsiao-Dong Chiang

Memorandum No. UCB/ERL M90/98

23 August 1990

(Revised 4 November 1990)

COVER PAGE

**BIFURCATION AND CHAOS IN
POWER SYSTEMS: A SURVEY**

by

Pravin Varaiya, Felix Wu,
and Hsiao-Dong Chiang

Memorandum No. UCB/ERL M90/98

23 August 1990
(Revised 4 November 1990)

ELECTRONICS RESEARCH LABORATORY

College of Engineering
University of California, Berkeley
94720

Bifurcation and Chaos in Power Systems: A Survey

Pravin Varaiya and Felix Wu
Department of Electrical Engineering and Computer Sciences
University of California, Berkeley, CA 94720

and
Hsiao-Dong Chiang
School of Electrical Engineering
Cornell University, Ithaca, NY 14853

PRELIMINARY DRAFT: PLEASE DO NOT QUOTE

23 August 1990
Revised 4 November 1990

*Work supported by EPRI Contract RP8010-8

**BIFURCATION AND CHAOS IN
POWER SYSTEMS: A SURVEY**

by

Pravin Varaiya, Felix Wu,
and Hsiao-Dong Chiang

Memorandum No. UCB/ERL M90/98

23 August 1990
(Revised 4 November 1990)

ELECTRONICS RESEARCH LABORATORY

College of Engineering
University of California, Berkeley
94720

TITLE PAGE

Contents

1	Introduction	6
2	Local bifurcation	9
2.1	Basic concepts	9
2.2	One generator model	10
2.3	Bifurcation of real power flow equations	15
2.3.1	Case $n = 2$	16
2.3.2	Bifurcation in the general case	17
2.3.3	Connection with catastrophe theory	18
2.3.4	Relation with transient stability	22
2.3.5	Limitations of the model	23
2.3.6	Practical implications	24
2.4	Bifurcation with reactive power flow	26
2.4.1	One generator model	26
2.4.2	The multi-generator case	32
2.4.3	Practical implications	35
3	Hopf bifurcation	36
3.1	The Hopf bifurcation theorem	36
3.2	Hopf bifurcation due to excitation control	39
3.3	Other Hopf bifurcations	43
3.4	Practical implications	44
4	Chaos	45
4.1	Basic concepts	45
4.1.1	Poincaré map	45
4.1.2	The homoclinic tangle	46
4.1.3	The Melnikov integral	53
4.2	Chaos in power systems	54

4.2.1	Chaos in a single machine I	54
4.2.2	A numerical study	56
4.2.3	Chaos in a single machine, II	56
4.2.4	Arnold diffusion	57
4.3	An appraisal of chaos in power systems	58
	Bibliography	59

List of Figures

1	Three phase portraits	9
2	Bifurcation diagram for (2)	10
3	Phase portrait in E	11
4	Phase portrait on α_0 , saddle connection	12
5	Phase portrait in EO	13
6	Phase portrait at β_0 , saddle-node bifurcation	13
7	Phase portrait in O	14
8	Local bifurcations for $n = 2$	16
9	The fold catastrophe	20
10	The cusp catastrophe	21
11	One generator supplying a PQ load	26
12	The power flow equations	27
13	Phase portrait of (25)	30
14	Phase portrait of (25) at bifurcation	31
15	Phase portrait of (25) after bifurcation	31
16	The Hopf bifurcation	38
17	IEEE Type 1 excitation system	40
18	The Poincare map	46
19	Heteroclinic and homoclinic saddle connections	47
20	Orbits of (38)	47
21	Breakup of homoclinic orbit	49
22	First correction	49
23	First correction	50
24	Homoclinic tangle	51
25	Trajectories of (34)	52
26	The Melnikov integral	53
27	Phase portrait of (41)	55

1 Introduction

The scientific literature on chaos and bifurcation has grown enormously since the publication of Lorenz's 1963 paper [1] showing chaotic motion in a simple, nonlinear, third order model that could be used for weather prediction. Advances in the understanding of bifurcation and chaos has come from the use of techniques of mathematical analysis, computer simulation, and laboratory experiments. Excellent and comprehensive accounts of the field are now available. The technical level of these accounts range from the mathematically difficult [2] to the widely accessible [3]. Treatments at intermediate levels of mathematical sophistication include [4, 5, 6, 7, 8, 9].

We do not provide another comprehensive view. Rather, we survey the published literature dealing with bifurcation and chaos in electric power systems. We also include a brief discussion of relevant mathematical concepts and results in order to make the presentation reasonably self-contained and accessible to power engineers. The objective of the survey is to determine the extent and significance of power systems behavior that can be understood by dynamic models exhibiting bifurcation and chaotic motion. Such a determination is, however, complicated by two factors.

The first factor applies in any attempt to describe a real phenomenon using the concepts of bifurcation and chaos. It has to do with the obvious point that these concepts refer to well-defined properties of a mathematical model (almost always a differential or difference equation); they do not refer in any direct way to the properties of the observed behavior of a real system. Therefore, assertions such as, "Voltage collapse is due to a saddle-node bifurcation," or "Turbulence in fluid flow is chaotic," mean first that there is a mathematical model (of power systems or fluid flow) whose behavior has the relevant mathematical property and, second, that there are scientific grounds for claiming that this is indeed a good model of the real system. This brings us to the second factor.

Clearly there is a strong basis for accepting the model if its behavior fits the observed data. Let us call such data 'direct' evidence. We should remind ourselves, however, of the intrinsic limitations of direct evidence since all measured data have finite granularity and extend over a finite time interval. But bifurcation and chaos refer to *asymptotic* properties of behavior – in the sense that the properties involve arbitrarily small differences in state and arbitrarily long intervals of time. Thus an unstable limit cycle and a fractal like the Cantor set are mathematical notions which can never be directly observed, and subjective judgement is involved whenever these properties are attributed to real systems. This judgement is of course conditioned by the extent, numerical accuracy, predictability, and reproducibility of the observations. The judgement will be more confident if, as in the case of fluid turbulence, data is based on controlled laboratory experiments; and the judgement will be more speculative if, as in the case of weather prediction, data is incomplete, sparse, infrequent, and the opportunity for experimentation is limited.

The case of power systems is a mixture of the examples of turbulence and weather prediction. At one end, we have controlled experiments with single generators so that we can be confident about models that predict certain electro-mechanical oscillations in generators.

At the other end, there are only anecdotal reports and spotty data on the few instances of power system failures that can be attributed to 'voltage collapse' and so at this stage one must be much less confident in an explanation of voltage collapse as, say, the result of a saddle-node bifurcation. The virtual absence of relevant direct evidence in power systems means that researchers have relied on what we call 'indirect' or second order evidence. This has forced researchers to analyze bifurcation and chaos in models that have been validated for quite different kinds of behavior. For example, we know that the swing equation model of a system of interconnected generators is useful in predicting the transient behavior of the system for a very short period (the so-called first swing period). Suppose now that the same swing equation model exhibits chaotic behavior which is an asymptotic property. How much confidence can we have in asserting that real power systems can exhibit chaotic motion?

We summarize these points. Power system models have been validated by observations over a certain range (direct evidence). But several of the predictions of bifurcation and chaos are based on model behavior over significantly different ranges. Our confidence can be increased only by further research – an issue which we address in a later report.

Our study is presented in three parts dealing with local bifurcations, Hopf bifurcations, and chaos. Local bifurcations arise when the number of equilibria changes. A Hopf bifurcation occurs when a periodic solution emerges from an equilibrium. Both these are 'local' phenomena since they are determined by the behavior of the model in a small neighborhood of an equilibrium. By contrast, chaos emerges from a global bifurcation, that is, a qualitative change in the phase portrait not restricted to a small neighborhood of an equilibrium. Typical examples of global bifurcations are homoclinic and heteroclinic bifurcations. As we shall see, both are encountered in power system models. Global bifurcation theory is incomplete and an active area of research in mathematics is concerned with developing techniques for global analysis.

Power systems are planned, designed and operated at a stable equilibrium point. Under normal conditions their behavior will not exhibit local or global bifurcation. Regions of the state space where these bifurcations occur, and the associated instabilities in behavior, are reached only under disturbances or unanticipated loading conditions. Nevertheless, the region of stable operating conditions is determined by the location of bifurcation. This makes the study of bifurcations important even for normal conditions.

Keeping in mind the reservations and qualifications mentioned above, we summarize our findings as follows.

1. The simplest differential equation models of power systems are so complex that they exhibit both local and global bifurcations. Local bifurcations can ultimately be traced to the fact that the power flow equations have multiple solutions.
2. In models that incorporate real power flow relations only (all load buses are PV buses), it seems that the capacity of transmission systems is so large relative to the flows that the local bifurcations although potentially present will not have practical significance.

3. However, power systems models in which voltages are determined by reactive power flows, these bifurcations can dramatically shrink the region of stability. Analytical and numerical studies of small scale systems indicate that the voltages can drop precipitously along unstable trajectories. This supports the claim that 'voltage collapse' is due to bifurcations. However, the phenomenon of voltage collapse is poorly documented in the published literature, and competing explanations cannot be ruled out in the current state of knowledge.
4. The electrical subsystem (exciter, transmission system) can interact with machine dynamics (swing equation) to produce oscillatory instabilities via a Hopf bifurcation. In practice this is likely to be a subcritical bifurcation and it reduces the region of stability.
5. The occurrence of global bifurcations leading to chaos has been demonstrated in models with unrealistic parameter values. These values have been chosen to simplify the analysis. Nevertheless, these studies do establish the presumption that chaotic behavior will exist in most power system models. It is not clear, however, if chaos occurs in regions of the state space sufficiently near operating regimes to affect the stability region to a significant extent.

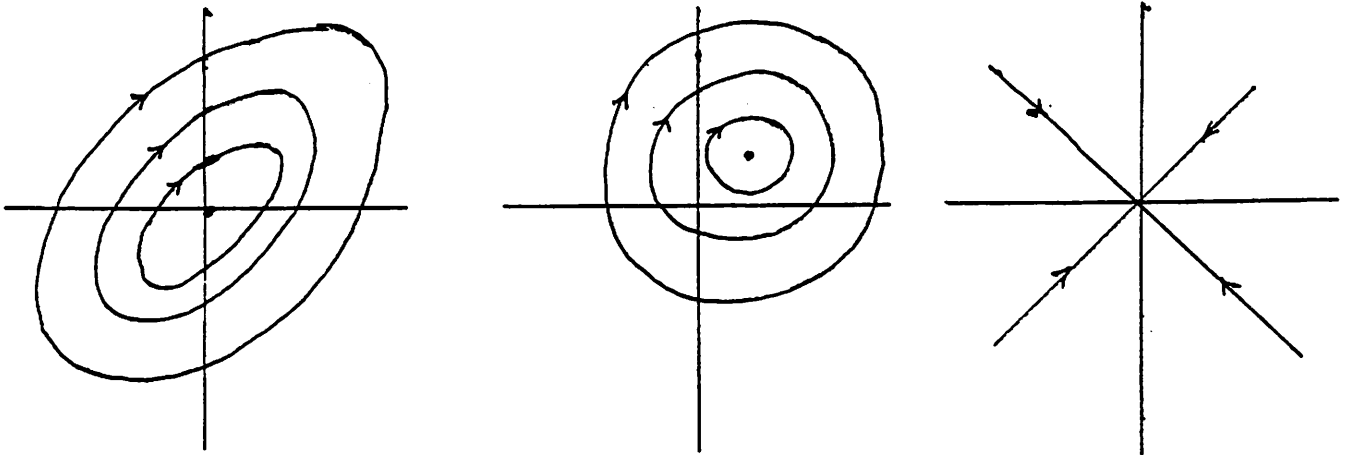


Figure 1: Three phase portraits

2 Local bifurcation

In this section we introduce the basic concepts of bifurcation. These concepts are illustrated by the important example of a swing equation model of a single generator connected to an infinite bus. We then survey power system models that show local bifurcation.

2.1 Basic concepts

Consider the differential equation system

$$\dot{x}(t) = f(x(t), \gamma) \quad (1)$$

where the state $x \in R^n$ and $\gamma \in R^p$ is a fixed parameter. The behavior of the system can be summarized by its *phase portrait* which is the set of all its orbits.¹ Different values of γ correspond to different systems and phase portraits. Our aim is to compare systems with different γ .

Two systems are said to be *topologically orbital equivalent* or TOE if their phase portraits can be continuously deformed into each other. This concept is meant to capture the intuitive idea that the behaviors of two systems can be qualitatively similar even though they are quantitatively different. Thus in Figure 1 the first and second phase portraits are TOE but the third is not.²

We return to (1). We will also say that two parameter values are TOE if the corresponding systems are TOE. A particular value γ_0 is said to be a *bifurcation point* of

¹An orbit is the locus of all points $\{x(t) \mid -\infty < t < \infty\}$ where $t \rightarrow x(t)$ is any trajectory of (1).

²Other definitions of topological equivalence have been proposed, see [8].

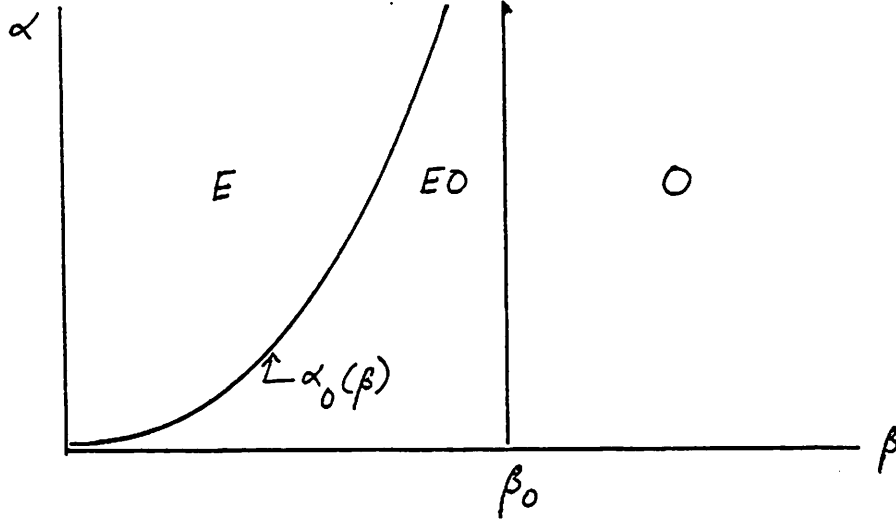


Figure 2: Bifurcation diagram for (2)

(1) if there exist parameter values arbitrarily close to γ_0 that are not TOE. The set of all bifurcation points is called the *bifurcation set*. We illustrate these concepts in an important example.

2.2 One generator model

The discussion below is based on [10, 11]. The swing equation model of a single generator connected to an infinite bus is given by

$$M\ddot{\theta} + D\dot{\theta} = P - B \sin \theta$$

where θ is the angle of the generator voltage relative to the bus voltage, P is the mechanical input power and $B \sin \theta$ is the electric power output; M, D are constants relating to the generator inertia and damping, B is related to the reactance of the lossless line connecting the generator and the infinite bus.

In state space form the equation becomes

$$\begin{aligned} \dot{\theta} &= \omega \\ M\dot{\omega} + D\omega &= P - B \sin \theta \end{aligned} \quad (2)$$

Two different state spaces will be used: either $(\omega, \theta) \in R^2$ or $(\omega, \theta) \in \Sigma = R \times S$ where $S = [0, 2\pi]$ is the unit circle and θ is measured modulo 2π .

Fix $B > 0$, and let $\alpha = D/M$, $\beta = P/M$. We compare the behavior of (2) for different values of $\gamma = (\alpha, \beta)$. The bifurcation diagram is given in Figure 2.

The parameter space is divided into three regions marked E , EO and O . Within each region the parameters are TOE. The regions are separated by the bifurcation set

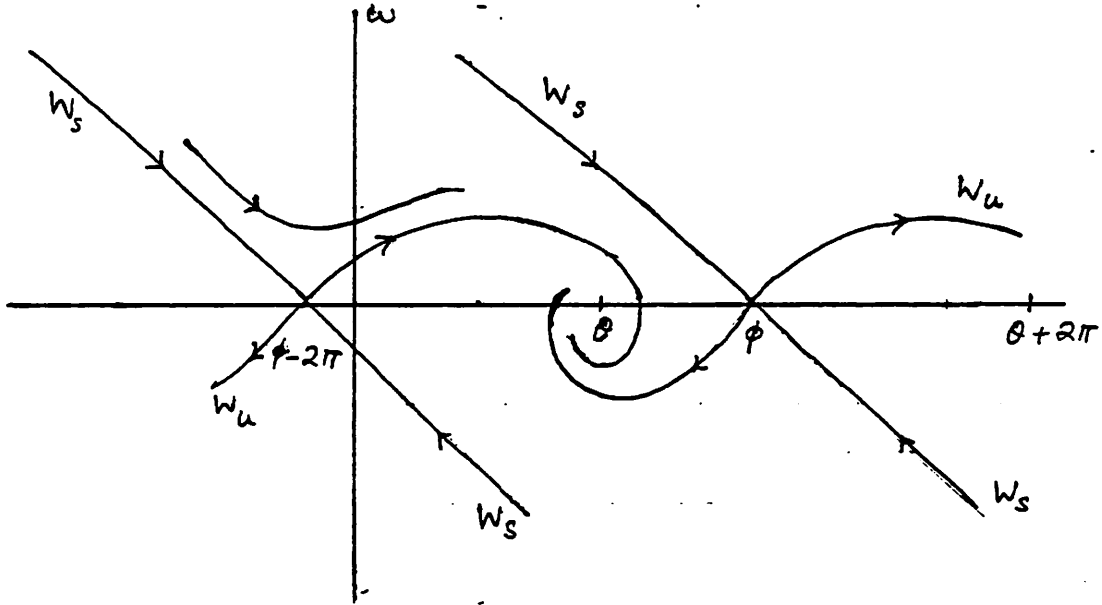


Figure 3: Phase portrait in E

consisting of the curve marked $\alpha_0(\beta)$ and the vertical line at β_0 . Note that the bifurcation set separates the TOE regions.

Suppose (α, β) is in E . There are two equilibria in Σ , namely, $(\omega = 0, \theta)$ and $(\omega = 0, \phi)$ where

$$\theta = \sin^{-1} \frac{M\beta}{B}, \quad \phi = \pi - \theta$$

In the state space R^2 there is an infinite number of equilibria displaced by multiples of 2π . The first equilibrium is a node and the second is a saddle.³ Every trajectory converges to one of these equilibria.⁴ The phase portrait for $\gamma \in E$ is shown in Figure 3. The state space is taken to be R^2 . If it were taken to be Σ , then the equilibrium at $\theta + 2\pi$ would coincide with θ and the equilibrium at $\phi - 2\pi$ would coincide with ϕ . The curves labeled W_s and W_u are the *stable* and *unstable manifolds* of the saddle.⁵ The regions bounded by W_s is the stability region or *attractor* of the stable equilibrium. Therefore, W_s is sometimes called the separatrix.

Decrease the damping α until $\alpha = \alpha_0(\beta)$ so γ is on the boundary of E . The phase portrait now changes to that of Figure 4. Since the phase portraits of Figures 3 and 4 are not TOE, points on α_0 are bifurcation points. One important feature should be noted. The

³An equilibrium is a node if the linearized differential equation has all its eigenvalues with strictly negative real part, it is a saddle if it has at least one eigenvalue with strictly negative real part and at least one with strictly positive real part.

⁴This is sometimes called complete stability.

⁵The stable manifold consists of all initial states from which trajectories converge to the saddle as $t \rightarrow +\infty$; the unstable manifold consists of all initial states from which trajectories converge to the saddle as $t \rightarrow -\infty$.

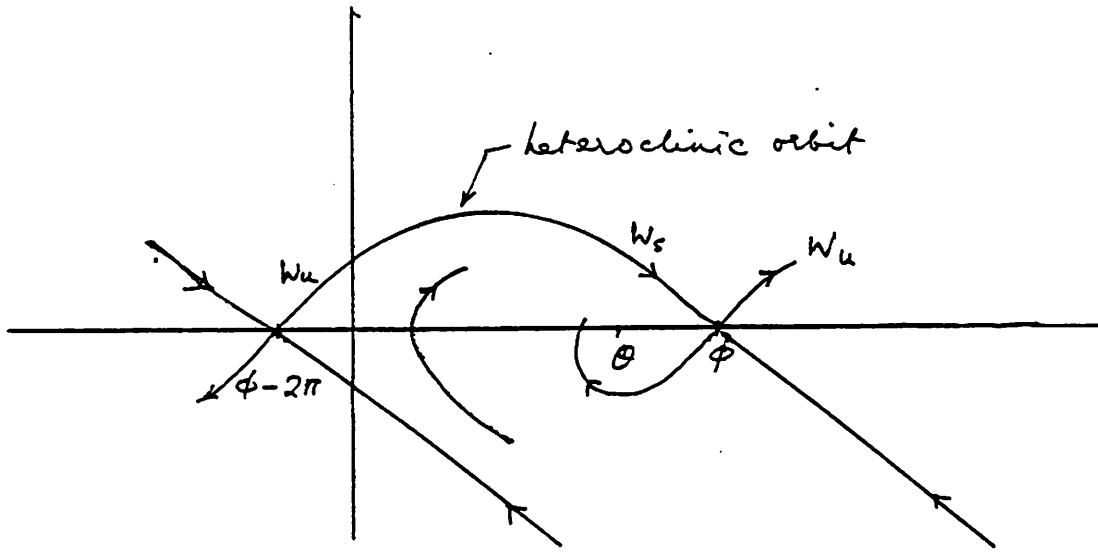


Figure 4: Phase portrait on α_0 , saddle connection

stable manifolds at the saddle at ϕ coincides with the unstable manifold of the saddle at $\phi - 2\pi$, and there is an orbit which connects these two saddles. Hence this bifurcation is called a *saddle connection* and the orbit is called a *heteroclinic orbit*. If we had taken Σ as the state space, ϕ and $\phi - 2\pi$ would be the same saddle, the orbit would connect the saddle to itself and it would be called a *homoclinic orbit*. We will see in §4 that this orbit can give rise to chaotic motion.

Decrease the damping still further so γ is in region EO . We get the qualitatively different phase portrait of Figure 5. The heteroclinic orbit has disappeared, and there appears a new asymptotic behavior marked by the curve C . In the state space Σ , C would correspond to a stable limit cycle.⁶ Physically, the generator is no longer in synchronism with the infinite bus.

Now increase β to $\beta_0 = B/M$. There is another qualitative change as the number of equilibria changes since $\theta = \phi$. The saddle and node fuse together and this is known as a *saddle-node bifurcation*. The phase portrait is given in Figure 6. Physically, this is the limit of steady-state stability and the point of maximum power transfer, $P = B$.

When $\beta > \beta_0$, there is no equilibrium.⁷ All solutions converge to the orbit C , as in Figure 7.

This lengthy discussion of the one generator case will suggest results for multi-generator systems where detailed calculations are not possible. We summarize a few conclusions which will be useful later on.

⁶The period of the limit cycle increases as α is decreased and the saddle connection could be thought of as a limit cycle with 'infinite' period.

⁷One says that the saddle and node have annihilated each other.

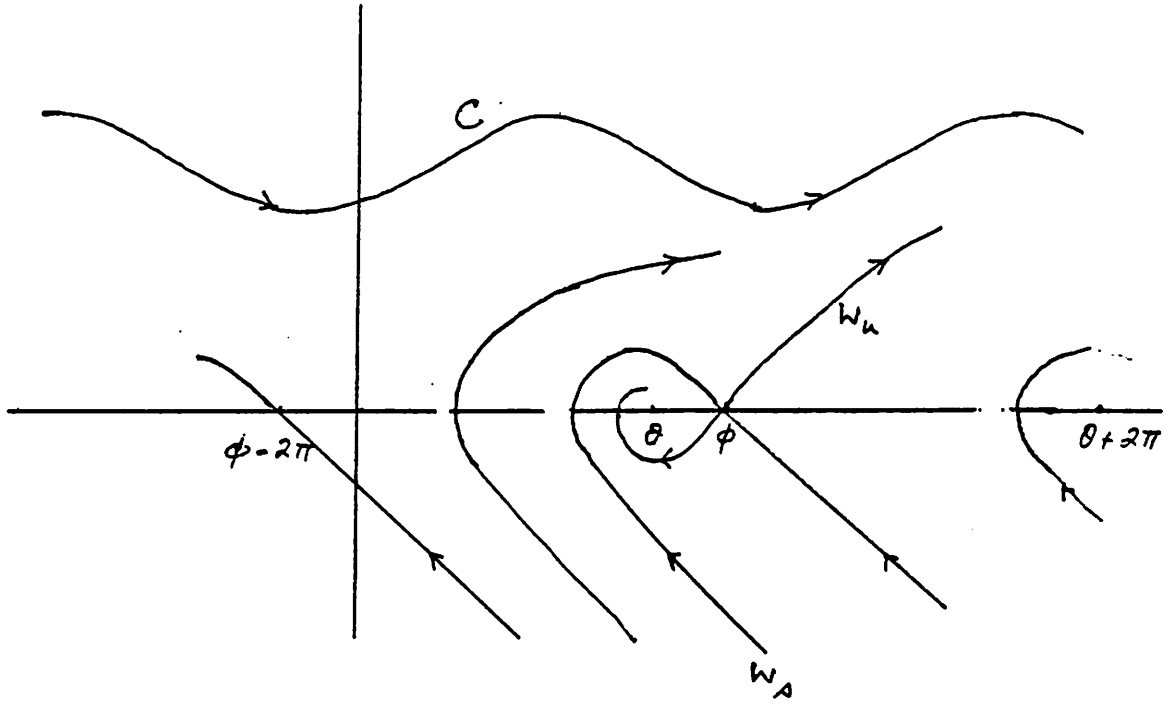


Figure 5: Phase portrait in EO

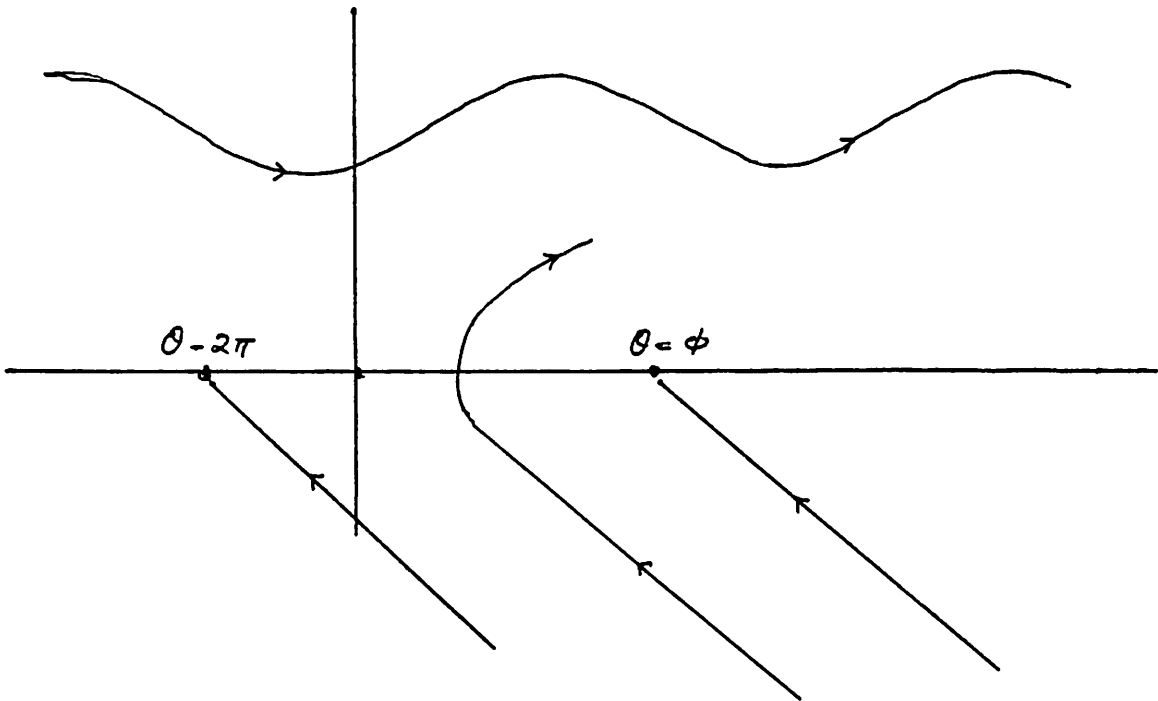


Figure 6: Phase portrait at β_0 , saddle-node bifurcation

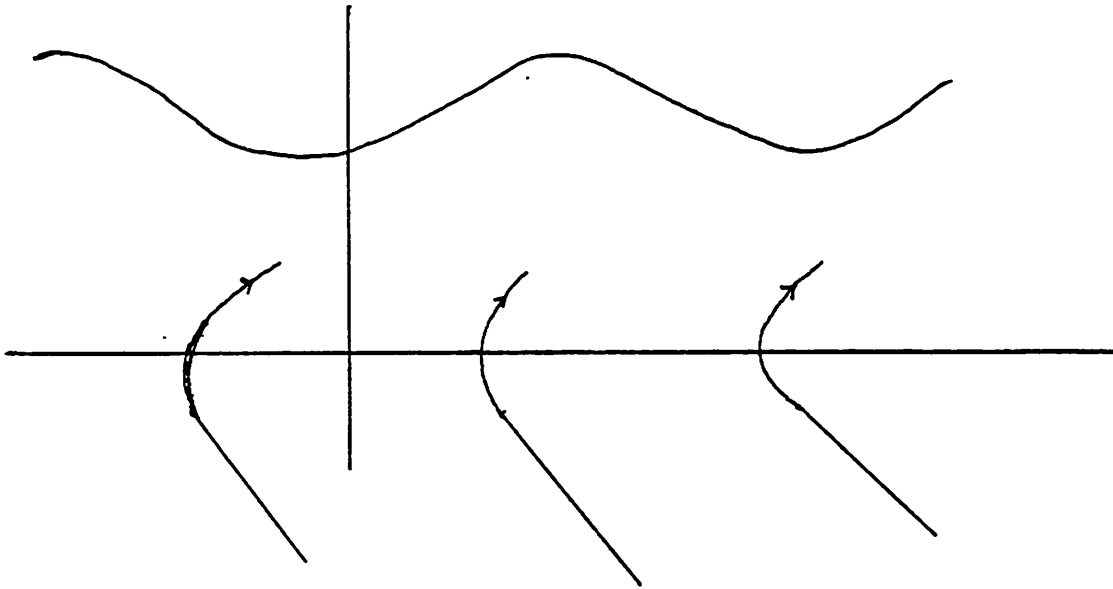


Figure 7: Phase portrait in O

First, the bifurcation set is a ‘thin’ region (measure 0) which separates the parameter space into ‘fat’ TOE regions (open sets). Sometimes, systems within each TOE region are said to be *structurally stable*.

Second, the saddle-node bifurcation is a special case of the more general bifurcation which occurs when there is a change in the number of equilibrium points. For the general model

$$\dot{x}(t) = f(x(t), \gamma)$$

we assume that the number of equilibria is finite. Then γ_0 is a bifurcation point if the number of equilibria changes as $\gamma \rightarrow \gamma_0$.⁸ This kind of bifurcation is very easy to check since a necessary condition is that for some equilibrium point x_0

$$\det \frac{\partial f}{\partial x}(x_0, \gamma_0) = 0 \quad (3)$$

i.e. the Jacobian at an equilibrium must become singular.⁹ Because this is a local condition, not requiring knowledge of the phase portrait, we say that γ_0 is a *local bifurcation point*. We study local bifurcations extensively in the remainder of this section.

Third, by contrast, the saddle-connection bifurcation is not caused by a change in the number of equilibria, and requires an analysis of the phase portrait. It is therefore called a *global bifurcation*. We will study these in connection with chaotic behavior.

⁸To see that γ_0 is indeed a bifurcation point, note that if two systems are TOE, then they must have the same number of equilibrium points.

⁹The necessity of (3) follows from the Implicit Function Theorem.

2.3 Bifurcation of real power flow equations

The single generator model (2) generalizes to a model for a n generator system,

$$\begin{aligned}\dot{\theta}_i &= \omega_i \\ M_i \dot{\omega}_i + D_i \omega_i &= P_i - f_i(\theta), \quad i = 1, \dots, n\end{aligned}\tag{4}$$

where

$$f_i(\theta) = \sum_{j=1}^{n+1} B_{ij} \sin(\theta_i - \theta_j)\tag{5}$$

Here $\theta_{n+1} \equiv 0$ is the reference angle of the voltage at the infinite bus; the parameters $B_{ij} = B_{ji} \geq 0$ if $i \neq j$ and $B_{ii} = 0$ are determined by the reactances of the lossless transmission lines connecting the generators.¹⁰

The state of the system is

$$(\omega, \theta) = (\omega_1, \dots, \omega_n, \theta_1, \dots, \theta_n) \in R^n \times R^n \text{ or } R^n \times \Sigma^n$$

If $\theta \in \Sigma^n = [0, 2\pi]^n$, then θ_i is measured modulo 2π . (ω, θ) is an equilibrium if and only if $\omega = 0$ and

$$f_i(\theta) = P_i, \quad i = 1, \dots, n\tag{6}$$

and it will be convenient to call θ an equilibrium if (6) holds. Equation (6) is called the *real power flow*. Let γ denotes the parameter vector of interest; it will consist of some of the P_i and some of the B_{ij} . A local bifurcation occurs at γ_0 if there is a change in the number of solutions of (6) at γ_0 . A necessary condition is that there is θ_0 such that

$$f(\theta_0, \gamma_0) = P, \quad \det F(\theta_0, \gamma_0) := \det \frac{\partial f}{\partial \theta}(\theta_0, \gamma_0) = 0\tag{7}$$

The Jacobian $F(\theta_0, \gamma_0)$ is symmetric, so all its eigenvalues are real. For future reference, recall the following fact.

Fact 2.1 [12] θ_0 is a stable equilibrium if and only if $F(\theta_0, \gamma_0)$ is positive definite. If $F(\theta_0, \gamma_0)$ has $l > 0$ negative eigenvalues, then $(\omega = 0, \theta_0)$ is a saddle and its unstable manifold has dimension l .

Take $\gamma = P$, the vector of net power injections, and let $N(P)$ be the number of equilibria of (4) or the number of solutions of (6). $N(P)$ takes values $0, 1, \dots$ and so P is a local bifurcation point if N is discontinuous at P . Alternatively, the set of local bifurcation points is the union of the boundaries of all sets of the form

$$R_k = \{P \mid N(P) = k\}, \quad k = 0, 1, \dots$$

We want to know what this set looks like. This turns out to be a rather difficult problem, and only some partial results are known. We review these.

¹⁰The simplifying assumptions underlying (4) are discussed later.

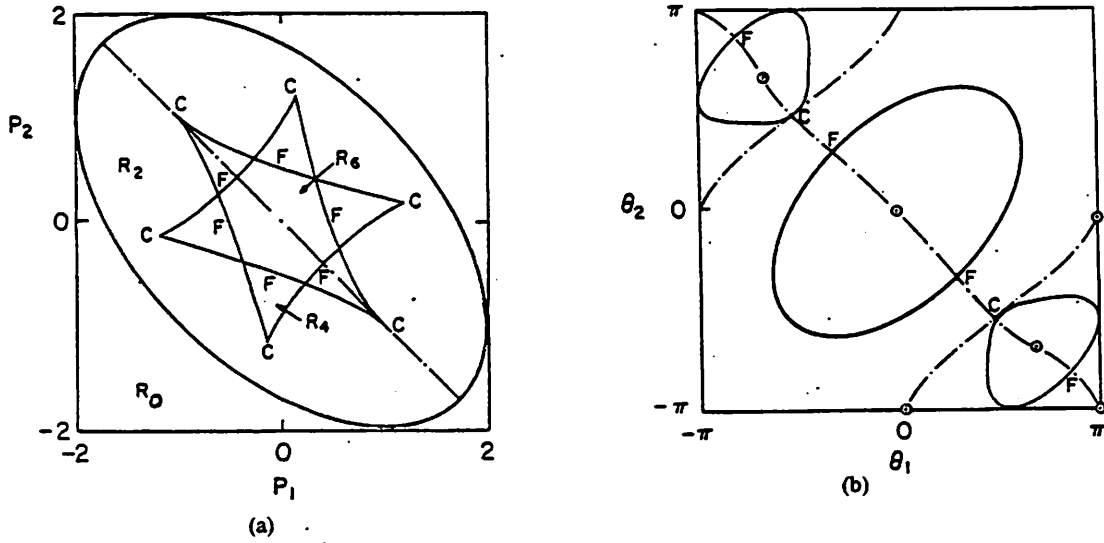


Figure 8: Local bifurcations for $n = 2$

2.3.1 Case $n = 2$

The case of $n = 2$ with symmetric interconnections, i.e. $B_{ij} = 1$, was first analyzed in [13]; more detailed work is reported in [14, 15, 16, 17]. The power flow equation becomes

$$\begin{aligned} P_1 &= \sin \theta_1 + \sin(\theta_1 - \theta_2) \\ P_2 &= \sin \theta_2 + \sin(\theta_2 - \theta_1) \end{aligned}$$

The (local) bifurcation diagram is given in Figure 8a. Figure 8b describes how the equilibrium points move as P moves along the diagonal dashed line in Figure 8a.

When P is in the open region labeled R_0, R_2, R_4 or R_6 there are 0, 2, 4, or 6 equilibria respectively. The boundaries of these regions comprise the bifurcation set and it consists of the oval and the star in Figure 8a.

When P is in the hexagon shaped region R_6 near $P = 0$ there are six equilibria. The six solutions for $P = 0$ are shown circled in Figure 8b where we have taken $\theta_i \in [-\pi, \pi]$ instead of $[0, 2\pi]$. Of the six equilibria, one is stable, the remaining five are saddles. As P moves from R_6 towards R_4 two of the saddles approach each other, they coincide when P enters the boundary of R_4 at F, and then they disappear (annihilate each other) when P enters R_4 . For reasons explained later this is sometimes called the *fold catastrophe* or bifurcation, hence the label F. Similarly, when P leaves the star shaped region R_4 , via any path except the corners labeled C, we have another fold bifurcation, two more saddles annihilate each other, so that in R_2 we have two equilibria, one of which is stable (node) and the other is a saddle. In case that P leaves R_4 via one of the corners labeled C, three of the saddles come together, and two of these get annihilated. This is called a *cusp catastrophe* or bifurcation. Finally, when P leaves R_2 there is a saddle-node bifurcation and there is no equilibrium in R_0 .

A better understanding of how the various equilibria come together can be obtained from Figure 8b which plots the locus of equilibria (the dashed lines) as P moves along the diagonal dashed line in Figure 8a. Note how three equilibria come together when P is at a cusp C.

Thus for the symmetric case, there are six equilibria for small values of $|P|$, and the number of equilibria decrease eventually to 0 as $|P|$ increases. Generally, the number decreases two at a time in a fold bifurcation. It is easy to see that the bifurcation diagram of Figure 8 is similar even in the non-symmetric case as long as the B_{ij} are not too different from each other; in particular the number of equilibria for $|P|$ small is six. It is surprising that as the B_{ij} become sufficiently different from each other, the number of equilibria for small $|P|$ suddenly changes to four (this is a bifurcation where the parameters are the B_{ij}), see [16].

One result for arbitrary B_{ij} is that if the load flow equation has a solution then it has a unique stable solution.¹¹ This is surprising since there is an example with $n = 4$ with two stable solutions [18], and an example with $n = 5$ where all solutions are unstable [14].

Finally we note an example in [15] showing a *global* bifurcation involving an orbit joining two saddles (heteroclinic orbit), similar to the case $n = 1$.

In summary, when we compare the case $n = 2$ with $n = 1$, we note new kinds of bifurcations (the cusp), a much more complex bifurcation set, and we find already that the complete bifurcation diagram is not known. It will not be surprising that our knowledge for the general case is very sketchy.

2.3.2 Bifurcation in the general case

Aside from some special examples mentioned above, the only general results are in [19] which we discuss next. The load flow equation

$$\sum_{j=1}^{n+1} B_{ij} \sin(\theta_i - \theta_j) = P_i, \quad i = 1, \dots, n \quad (8)$$

can also be expressed as the system of polynomial equations

$$B_{in+1}x_i + \sum_{j \neq i} B_{ij}(x_i y_j - x_j y_i) = P_i, \quad i = 1, \dots, n \quad (9)$$

$$x_i^2 + y_i^2 = 1, \quad i = 1, \dots, n \quad (10)$$

by using $x_i = \sin \theta_i$, $y_i = \cos \theta_i$. Observe that for $P = 0$, there are at least 2^n solutions given by $x_i = 0$, $y_i = \pm 1$, corresponding to $\theta_i = 0$ or π .

Suppose we regard the x_i, y_i as *complex* variables.

Fact 2.2 [19] The number of complex solutions to (9), (10) is $\binom{2n}{n}$.

¹¹The uniqueness of the stable equilibrium is established in [15] and in [16].

Since only real solutions of (9), (10) correspond to solutions of (8), we have the following bounds for the number N_n of load flow solutions,

$$2^n < N_n < \binom{2n}{n}$$

It is conjectured in [19] that the upper bound is tight. The following table gives some values.

n	2	3	4	5	6	7
lower bound	4	9	16	25	36	49
upper bound	6	20	70	252	924	3432

Practical power systems have tens of generators and so the real load flow solutions number in the thousands (!!). Therefore the local and global bifurcations in practical power systems are extremely complex. We address the significance of this fact later on.

2.3.3 Connection with catastrophe theory

The real power flow equation can also be expressed as

$$\frac{\partial V}{\partial \theta}(\theta, \gamma) = 0$$

where the ‘potential’ V is given by

$$V(\theta, \gamma) = - \sum_{i < j} B_{ij} \cos(\theta_i - \theta_j) - \sum_{i=1}^{n+1} P_i \theta_i \quad (11)$$

(Recall that $\theta_{n+1} \equiv 0$ and the parameter vector γ consists of some of the P_i and B_{ij} .) Thus the load flow solutions are critical points of V .¹² From Fact 2.1 we note that the critical points which are local minima of V are stable solutions; the rest are saddles. A critical point θ is *degenerate* if

$$\det \frac{\partial^2 V}{\partial^2 \theta}(\theta, \gamma) = 0$$

Finally, the *catastrophe set* of V is the set of all parameters γ which have a degenerate critical point. Comparing this with (7), we see that the catastrophe set is the same as the local bifurcation set.¹³

This identification permits the use of catastrophe theory [20]. To appreciate the theory first recall a theorem of Morse [21]. Suppose θ_0 is a *non-degenerate* critical point for γ_0 and suppose the Hessian matrix

$$\frac{\partial^2 V}{\partial^2 \theta}(\theta_0, \gamma_0) \quad (12)$$

¹²Critical points are points where the gradient of V vanishes.

¹³This is not strictly correct since (7) is only a necessary condition for bifurcation.

has n_+ positive and n_- negative eigenvalues, $n_+ + n_- = n$. Then there exists a smooth coordinate change $\theta \rightarrow x$ and $\gamma \rightarrow a$ from a neighborhood of (θ_0, γ_0) onto a neighborhood of $(0, 0)$ such that in the new coordinates V has the form

$$V(\theta, \gamma) - V(\theta_0, \gamma_0) \sim \sum_{i=1}^{n_+} x_i^2 - \sum_{i=1}^{n_-} x_{n_+ + i}^2$$

Thus V is a definite quadratic form near a non-degenerate critical point and is completely determined by the number of positive and negative eigenvalues. When the critical point is degenerate the situation is much more complex. We present the most useful result.

Suppose $\gamma \in R^p$, $p \leq 5$. Let θ_0 be a degenerate critical point and suppose the Hessian (12) has n_+ positive, n_- negative, and n_0 zero eigenvalues. Suppose n_0 is 1 or 2. Then there exists a smooth coordinate change $\theta \rightarrow x$ and $\gamma \rightarrow a$ from a neighborhood of (θ_0, γ_0) onto a neighborhood of $(0, 0)$ such that in the new coordinates V has the form

$$V(\theta, \gamma) - V(\theta_0, \gamma_0) \sim \text{Cat}(n_0, p) + \sum_{i=1}^{n_+} x_{n_0 + i}^2 - \sum_{i=1}^{n_-} x_{n_0 + n_+ + i}^2 \quad (13)$$

Here $\text{Cat}(n_0, p)$ is one of 11 polynomials in x_1, \dots, x_{n_0}, p of whose coefficients are the parameters a_1, \dots, a_k . These polynomials are called the *elementary catastrophe functions*. They were first described by Thom [22]. (The discussion here is adapted from [20].)

The most important conclusion to be drawn from (13) is that the catastrophe set is determined entirely by the Cat functions since the other two terms are strictly quadratic. As a result, in a neighborhood of (θ_0, γ_0) the critical points and the catastrophe set depend only on (x_1, \dots, x_{n_0}) and a . This can be a tremendous simplification since the dimension of θ , n , can number in the tens while n_0 can be very small. We illustrate this with two examples.

In the first example, $n_0 = p = 1$,

$$\text{Cat}(1, 1) = a_1 x_1 + \frac{1}{3} x_1^3$$

so the degenerate critical points are given by

$$\frac{d\text{Cat}(1, 1)}{dx_1} = a_1 + x_1^2 = 0 \text{ and } \frac{d^2\text{Cat}(1, 1)}{d^2x_1} = 2x_1 = 0$$

The catastrophe set consists of a single point $\{a_1 = 0\}$. As can be seen in Figure 9, when $a_1 < 0$ there are two critical points which come together as $a_1 \rightarrow 0$, and disappear for $a_1 > 0$. This is the *fold catastrophe*.

In the second example, $n_0 = 1$, $p = 2$,

$$\text{Cat}(1, 2) = a_1 x_1 + \frac{1}{2} a_2 x_1^2 + \frac{1}{4} x_1^4$$

The catastrophe set is given by

$$\frac{d\text{Cat}(1, 2)}{dx_1} = a_1 + a_2 x_1 + x_1^3 = 0 \text{ and } \frac{d^2\text{Cat}(1, 2)}{d^2x_1} = a_2 + 3x_1^2 = 0$$

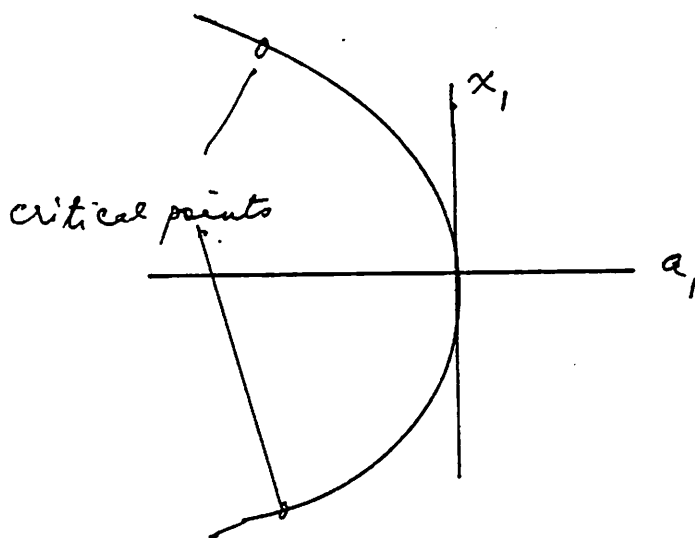


Figure 9: The fold catastrophe

which gives

$$3a_1^2 + a_2^3 = 0$$

Figure 10 shows the *cusp catastrophe*. There are three critical points when a is inside the ‘cusp’ and one critical point outside. It is interesting to note how the cusp catastrophe is ‘built up’ from two folds.

We have already encountered these two catastrophes in §2.3.1. In practice, the result on elementary catastrophes can be easily used in a qualitative way since it only requires knowing the dimension of the null space of the Hessian (12). It is, however, very difficult to use quantitatively since it requires calculation of the nonlinear transformation of coordinates $(\theta, \gamma) \rightarrow (x, a)$. This transformation depends on derivatives of V of order ≥ 3 .

This difficulty is illustrated in the series of papers [23, 24, 25, 26, 27, 28, 29]. The basic idea is the same in all of these. For example in [23], the potential (11) is derived for a single generator so there is a single variable, θ_1 ; the γ parameter vector include power demand, transmission line admittance, generator reactance, etc. Thom’s theorem is invoked to assert that the potential can be transformed into the fourth order polynomial $\text{Cat}(1,2)$ above, so that one obtains the cusp catastrophe. However, this is not very interesting since the relation between the transformed parameters (a_1, a_2) and the original parameters is not established, so one can not obtain any physically meaningful interpretation of the catastrophe result. The other papers extend the discussion to the multi-generator cases. These papers contain two errors which may be worth pointing out.

The first error has to do with the fact that their models permit resistive (rather

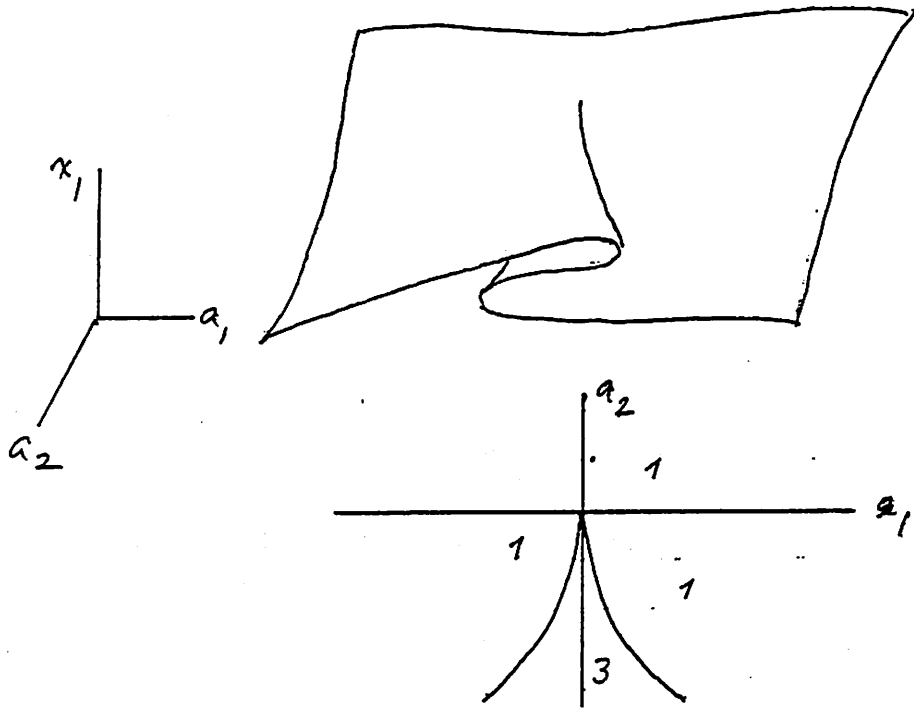


Figure 10: The cusp catastrophe

than lossless) transmission lines in which case the real power flow equation becomes

$$\sum_{j=1}^{n+1} B_{ij} \sin(\theta_i - \theta_j) + \sum_{j=1}^{n+1} C_{ij} \cos(\theta_i - \theta_j) - P_i = 0, \quad i = 1, \dots, n \quad (14)$$

instead of (8). (Here $C_{ij} = C_{ji}$, $C_{ii} = 0$.) But this system of equations *can not* be put into the form

$$\frac{\partial V}{\partial \theta}(\theta, \gamma) = 0$$

as can be seen by noting that the Jacobian of (14) is not symmetric.¹⁴

Therefore catastrophe theory results can not be used.

The second error has to do with their attempt to relate the potential to transient stability. Since this discussion is not directly connected with the main objective of this survey we present it as a separate subsection and the reader may omit it entirely with no loss in continuity.

2.3.4 Relation with transient stability

To understand the relation, use (11) to rewrite (4) as

$$\begin{aligned} \dot{\theta}_i &= \omega_i \\ M_i \dot{\omega}_i + D_i \omega_i &= -\frac{\partial V}{\partial \theta_i}, \quad i = 1, \dots, n \end{aligned} \quad (15)$$

Define the ‘energy’ function $W(\omega, \theta)$ by

$$W(\omega, \theta) = \frac{1}{2} \sum_i M_i \omega_i^2 + V(\theta) \quad (16)$$

It is customary to call the first term on the right the ‘kinetic’ energy and the second term the ‘potential’ energy. The interpretation is reinforced by calculating the rate of change of energy along any trajectory of (15),

$$\frac{dW}{dt} = \sum \frac{\partial W}{\partial \omega_i} \dot{\omega}_i + \sum \frac{\partial W}{\partial \theta_i} \dot{\theta}_i = -\sum D_i \omega_i^2$$

For future reference note that if there is no damping ($D_i = 0$), then $W = \text{constant}$ along every trajectory, so W is a *first integral* of (15). If damping is present, then W decreases along every trajectory and so it can serve as a Lyapunov function.

The argument about transient stability proceeds as follows. Suppose the system undergoes a fault, and let (ω, θ) be the initial state when the fault clears. Let $(\omega_0 = 0, \theta_0)$

¹⁴The question of existence of a Lyapunov function for lossy transmission lines is not yet fully resolved. [30] shows that such a function cannot be obtained by a smooth transformation of a Lyapunov function for lossless lines; however [31] provides a local energy-like Lyapunov function for lossy lines. Lastly, [32] shows that there cannot always exist an energy function for lossy lines, and exhibits, for the case of small losses, a local energy function which can be incorporated into direct stability analysis.

be a stable post-fault equilibrium. We want to determine whether (ω, θ) is in the (transient) stability region of (ω_0, θ_0) , i.e. whether the post-fault trajectory starting at (ω, θ) will converge to (ω_0, θ_0) .

Note that since $\omega_0 = 0$,

$$W(\omega_0, \theta_0) = V(\theta_0)$$

and, as we observed earlier, θ_0 is a strict local minimum of V . Let V_{max} be the value of V at a local maximum ‘near’ θ_0 .¹⁵ Then it is asserted that (ω, θ) is in the stability region provided that

$$W(\omega, \theta) < V_{max}$$

Unfortunately this is not correct. The precise relation is more delicate and is fully discussed in [33].

2.3.5 Limitations of the model

The preceding argument leads to the conclusion that the swing equation model (4), (5) must lead to numerous bifurcations. We now address the question whether this conclusion will stand when the simplifying assumptions are removed.

The most general models also have the form

$$\begin{aligned} \dot{\theta}_i &= \omega_i \\ M_i \dot{\omega}_i + D_i \omega_i &= P_i - P_i^e, \quad i = 1, \dots, n \end{aligned} \tag{17}$$

where P_i is the mechanical power input and P_i^e is the electric power output at the i th generator. The differences between the models have to do with how P_i^e and P_i are determined. We list some of the major differences. Since

$$P_i^e = \text{Re} V_i I_i^*$$

where V_i, I_i are the terminal voltage and current, these differences have to do with how these are determined.

- In the model considered above the $V_i = \text{constant}$, and the I_i are determined by a lossless reduced admittance matrix.¹⁶ This results in the expression (5). The model is a good predictor of transient behavior over a very short time interval – the so-called ‘first swing’ period, which is on the order of a few seconds.
- A slightly more general model allows a lossy reduced admittance matrix and P_i^e is now given by (14). This permits loads to be modeled as impedances. As we have seen, one

¹⁵The precise meaning of ‘near’ depends on the author. Since a local maximum is at a critical point of V , it is at an unstable equilibrium point (uep), and authors have variously selected ‘closest uep’, ‘relevant uep’, etc.

¹⁶The reduced admittance matrix is a characterization of the transmission network and the loads as seen from the n generator terminals, see [34].

can no longer write P^e as the gradient of a potential. Catastrophe theory can not be used. But the more general Lyapunov-Schmidt procedure [35] is applicable as shown in [14]. Although the details have not been worked out, it is clear that the kinds of bifurcations described above will persist. Moreover, as shown in [36], a new kind of bifurcation – the Hopf bifurcation is now possible.

- The one-axis generator model assumes constant terminal voltage, distinguishes it from the internal generator voltage, and incorporates flux decay effects [37]. The dimension of the state for a single generator is now increased by one. As shown in [38], however, the resulting dynamics can still be expressed using a more complicated potential energy function. Again, although the details are not worked out, it is clear that the bifurcations will persist.
- The loads in [39] are viewed as PV buses, as PQ buses in [38], while [40] allows more general loads with constant real power demand and voltage-dependent reactive power demand. These are considered more accurate than constant impedance loads. In all these cases there exists a potential energy function, bifurcations persist, and analysis using catastrophe theory is possible..
- In order to predict transient behavior over a longer time interval, it is necessary to include the dynamics of the voltage regulator which determines the generator terminal voltage. The dimension of the state space increases by two or three depending on the regulator model [37]. Nevertheless the core swing equations remain and so should the bifurcations. New kinds of bifurcation also appear [36].
- Over even longer time intervals, the mechanical input power vector, P , can not be considered constant, since the action of the governor and AGC come into play. The nature of the bifurcations in these models has not been worked out.
- Finally, none of these models includes the effect of protection systems. The resulting models would include discrete changes in network topology. These are no longer differential equation models and it is likely that only numerical analysis can be carried out.

In summary, one can be very confident that the bifurcations predicted on the basis of the ‘classical’ swing equation model (4), (5) will be present in more realistic models and the additional complexity will only introduce additional bifurcations. The question remains whether the bifurcations are important in practice. That question is addressed next.

2.3.6 Practical implications

The preceding discussion has established the occurrence of bifurcations that in the final analysis derive from the multiplicity of solutions to the real power flow equation which we write as

$$\frac{\partial V}{\partial \theta}(\theta, \gamma) = 0$$

However these bifurcations may not be important in practice if they occur in regions where the power system never operates. To make this precise define the *bifurcation manifold* by

$$\text{BM} = \{(\theta, \gamma) \mid \frac{\partial V}{\partial \theta}(\theta, \gamma) = 0 \quad \det \frac{\partial^2 V}{\partial \theta^2}(\theta, \gamma) = 0\} \subset R^n \times R^p$$

and define the *operating region*

$$\text{OR} = \{(\theta, \gamma) \mid \frac{\partial V}{\partial \theta}(\theta, \gamma) = 0, (\theta, \gamma) \text{ is a possible stable operating point}\}$$

If OR and BM are disjoint and sufficiently far apart, then the potential bifurcations will not be observed in practice. Since OR depends on operating procedures, judgment is involved in making a determination.

Consider first the one generator case of §2.2. Suppose M, D, B are fixed, and the input power, P , is the parameter. Then OR consists of the pairs (θ, P) where $\theta = \sin^{-1} P/B$. From Figure 2 we see that if P/B is sufficiently smaller than 1, then the saddle node bifurcation will be avoided. In practice $P/B \ll 1$, equivalently $\theta \ll \pi/2$, and so we may say that this bifurcation will not be observed. (This is equivalent to saying that steady-state instability will not be observed.) However, since damping is usually very small, the parameter is in the region EO . Therefore, a transient, caused for instance by a fault, can lead to the loss of synchronism due to the saddle-connection bifurcation. The loss of synchronism is a transient instability – a phenomenon observed in practice.

For the general case of (4), (5) the following result is relevant. The first part is proved in [13, 14]. The second assertion is proved in [39, 14].

Fact 2.3 Let θ be an equilibrium such that

$$|\theta_i - \theta_j| < \pi/2 \text{ whenever } B_{ij} > 0 \tag{18}$$

Then θ is a stable operating point. Moreover, the function $f(\theta)$ is one-to-one in this region.

In practice, real power transmission capacity is so large compared to the flow that angle differences at operating points do satisfy (18), so we can conclude that local bifurcations are unlikely to be observed. However, oscillatory instabilities arising from saddle-connection bifurcations can indeed occur during a transient as in the single generator case. But we must keep in mind that the possibility of these bifurcations has not been established for $n > 2$ and only one example for the case $n = 2$ is known. This remains a significant unanswered question.

In summary we can draw the following conclusions.

- Local bifurcations of the real power flow equation are not significant if power systems are operated well within steady-state stability limits (formally defined by (18)). There is an important exception: as we will see in the next section, the reactive power balance constraint can reduce the real power flow transmission capacity significantly to lead to steady-state instability.
- Saddle-connections bifurcations, which we suspect are always present, can create oscillatory instabilities that are observed in a transient. In fact, as we will see in §4, these can even lead to chaotic behavior.

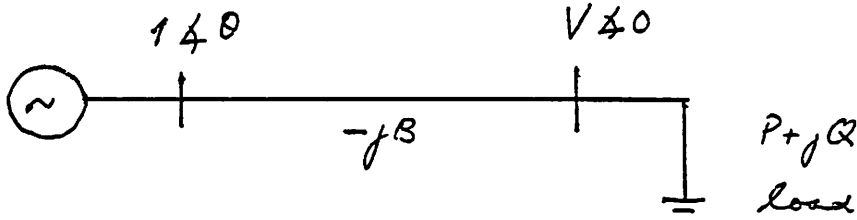


Figure 11: One generator supplying a PQ load

2.4 Bifurcation with reactive power flow

We continue the study of local bifurcation, extending the model to include reactive power balance. The analysis is similar to that carried out above, although the details are more complex. Several researchers have claimed that these local bifurcations explain ‘voltage collapse’. This claim is evaluated. We start with the case of a single generator.

2.4.1 One generator model

Consider a single generator supplying a PQ load over a lossless transmission line as in Figure 11. The generator voltage is $V_1 = 1e^{j\theta}$, the load bus voltage $V_2 = Ve^{j0}$ is taken as reference. The line admittance is $-jB$ and the load complex power demand is $P + jQ$ ($P > 0$, $Q > 0$).

The complex power injected into the network at the generator bus is

$$BV \sin \theta + jB(1 - V \cos \theta)$$

The complex power injected into the network at the load bus is

$$-BV \sin \theta - jB(V \cos \theta - V^2) = -P - jQ$$

which gives the power flow equations

$$0 = P - BV \sin \theta \tag{19}$$

$$0 = Q - BV \cos \theta + BV^2 \tag{20}$$

Let P_m be the mechanical power input. Generator dynamics are given by the swing equation

$$M\ddot{\theta} + D\dot{\theta} = P_m - BV \sin \theta \tag{21}$$

Equations (19)-(21) is our initial model.

We first analyze the power flow equations (19), (20). Figure 12 gives a sketch of the two equations. There are two solutions (θ, V) marked s, u where both equations are

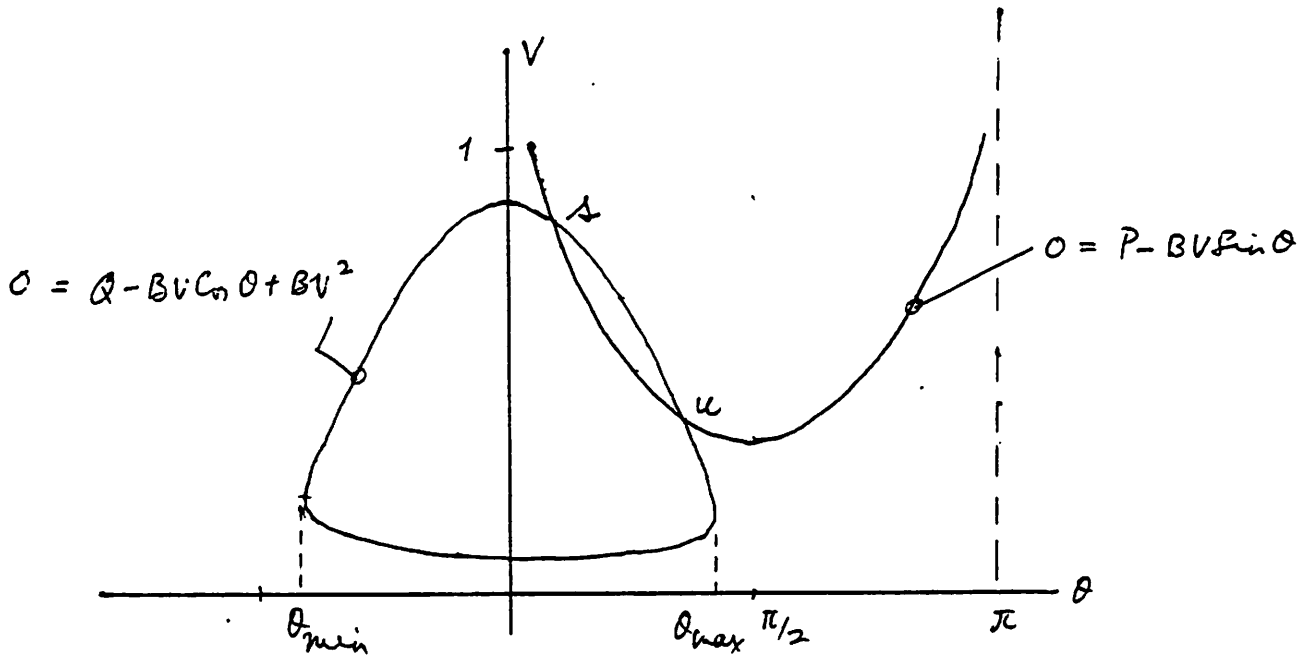


Figure 12: The power flow equations

satisfied. Note that as P increases the U-shaped curve moves up, and as Q increases the closed curve shrinks. Therefore, as P or Q increases, the solutions s and u approach each other, coincide and, beyond that, there is no solution. We will see later in the general case that this phenomenon can be seen as a fold catastrophe or a saddle-node bifurcation.

The initial model (19)-(21) is over-determined since (19), (20) by themselves alone admit at most two solutions and there is no 'room' for the differential equation to evolve. The model must be relaxed. We present one option now, and another option in the general case.

In the first option, the real power flow relation, (19), is only required to hold in equilibrium while (20) is required to hold at all times.¹⁷ So we must have $P_m = P$ and the model

$$M\ddot{\theta} + D\dot{\theta} = P - BV \sin \theta \quad (22)$$

$$0 = Q - BV \cos \theta + BV^2 =: f(\theta, V) \quad (23)$$

The analysis of this constrained differential equation needs some care. The state space is taken to be $(\omega, \theta, V) \in R \times \Sigma$ where Σ is the set of all (θ, V) satisfying (23). From Figure 12 we see that Σ is the 1-dimensional manifold given by the closed curve. When $(\theta, V) \in \Sigma$ and $\partial f / \partial V(\theta, V) \neq 0$, which requires $\theta_{min} < \theta < \theta_{max}$, we can solve (23) to obtain V as a function of θ , substitute it into (22), and obtain an ordinary differential equation in θ . Thus, starting at any initial state $(\omega, \theta, V) \in R \times \Sigma$, we get a well-defined trajectory

¹⁷For instance, this approach is used in the example in [41].

so long as $\theta \in (\theta_{min}, \theta_{max})$. Once the boundary is reached, however, the trajectory can no longer be extended.¹⁸

$(\omega = 0, \theta, V)$ is an equilibrium if (19, 20) hold. We will also call (θ, V) an equilibrium. If the two curves in Figure 12 intersect as shown there are two equilibria, namely s and u . It is easy to check that s is stable (node) and u is a saddle. As P or Q increase, the two equilibria will coincide in a saddle-node bifurcation, and then they disappear. Many researchers have pointed to this as an explanation of voltage collapse. We examine this a bit further to point out some misunderstandings in the literature.

Observe that an increase in P as well as an increase in Q will cause the bifurcation. Bifurcation due to increases in P are said to be due to the inability of the system to supply more real power, and bifurcations due to increases in Q can be said to be due to its inability to supply reactive power. As we have seen, these are *not* alternative explanations; each is only a partial description of what is happening.

The occurrence of bifurcation is signaled by the vanishing of the determinant of the Jacobian of the power flow equation.¹⁹ Taking the differential of (19), (20) gives

$$\begin{bmatrix} BV \cos \theta & BV \sin \theta \\ -BV \sin \theta & B \cos \theta - 2BV \end{bmatrix} \begin{bmatrix} d\theta \\ dV \end{bmatrix} = \begin{bmatrix} dP \\ dQ \end{bmatrix} \quad (24)$$

At the bifurcation the determinant vanishes and one can not always solve for $(d\theta, dV)$ in terms of changes in the demand (dP, dQ) .²⁰

The diagonal terms in (24) are non-zero at the bifurcation. So one can solve for dV from the second equation in (24) and substitute in the first equation to get

$$d\theta = \frac{(B \cos \theta - 2BV)dP - BV \cos \theta dQ}{\Delta}$$

where Δ is the determinant. Since $\Delta = 0$, [41], following [44], refers to this as “infinite sensitivity” of the “angle variables” and associates this with the “loss of steady-state stability.” On the other hand, we can also solve for $d\theta$ from the first equation in (24) and substitute in the second equation to get

$$dV = \frac{BV \sin \theta dP + BV \cos \theta dQ}{\Delta}$$

Since $\Delta = 0$, [41] states that “this bifurcation is associated with infinite sensitivity of the load voltage magnitudes ... This property is the essential feature of so-called voltage collapse.” However, as we have seen, that the characterizations of ‘infinite sensitivity of angle variables’ and ‘infinite sensitivity of voltage magnitudes’ are not mutually exclusive. *In fact, both are likely to occur simultaneously and so such characterizations are either partial or misleading.* We can assert only that the bifurcation is preceded by a coalescence

¹⁸The trajectory can be extended via singular perturbations, [42].

¹⁹It is worth repeating that the vanishing of the determinant is necessary but not sufficient for bifurcation.

²⁰The vanishing of the determinant as signaling a loss of steady-state stability was noted in [43], while [44, 45] point to it as a cause of voltage instability.

of two power flow solutions, and that it leads to a loss of (transient) stability. From Figure 12 we can infer that if B is increased, the U-shaped curve moves down and the closed curve expands. Hence a greater value of B (which means smaller inductance or smaller length) will reduce the chances of bifurcation.

We now make a preliminary evaluation of the claim that this bifurcation is a cause of ‘voltage instability’. The claim is succinctly stated for example in [46]: “The voltage stability problem ... is associated with the increased loading of long distance transmission lines and the insufficient local reactive power supply.” The lack of sufficient transmission capacity is noted in [47]: “Transmission facilities [in the New York Power Pool] have increased by 21 percent from 1975 to 1988 but are only expected to increase by 2 percent by the year 2000. ... I believe the situation in New York is typical of many systems throughout the country. ... It means that in the foreseeable future, the transmission network will become more heavily loaded. Transfers of power over greater distances will be required ...” The author goes on to quote a recent NERC report according to which these heavy transfers ‘will load the transmission network above surge-impedance levels more often so that at times transmission lines will act as reactive loads rather than sources of reactive power.’

Several papers relate voltage collapse to the vanishing of the determinant of the Jacobian of the power flow equations or, equivalently, to the vanishing of one of its eigenvalues; indices and algorithms have been proposed for use in on-line security analyses to signal the onset of voltage collapse, e.g. [43, 44, 48, 49, 50]. Others have gone further to claim that the voltage collapse is related to the occurrence of two power flow solutions that are very close to each other, e.g. [51, 46].²¹

The single generator study above, together with the multi-machine case discussed in the next subsection, lend support to the claim that a local bifurcation leads to voltage collapse. However, as we saw in §2.2, instabilities can be caused by global bifurcations as well. We examine this possibility next.

From Figure 12 we see that if $\theta_{min} < \theta < \theta_{max}$, we can solve (23) for V uniquely in terms of θ .²² Denote this solution as $V = V(\theta)$; note that $V(\theta) = V(-\theta)$ and $V(\theta)$ decreases as $|\theta|$ increases. Substituting for V in (22) gives

$$\begin{aligned} \dot{\theta} &= \omega \\ M\dot{\omega} + D\omega &= P - BV \sin \theta \end{aligned} \tag{25}$$

This model is valid for

$$(\omega, \theta) \in R \times (\theta_{min}, \theta_{max})$$

There are two equilibria, θ_s and θ_u , corresponding to s and u in Figure 12. θ_s is stable and θ_u is a saddle. Note that

$$P - BV \sin \theta > 0 \Leftrightarrow \theta > \theta_u \text{ or } \theta < \theta_s$$

From this we obtain the phase portrait of (25) sketched in Figure 13.

²¹We should point out that competing explanations for voltage instability include those due to the behavior of transformer tap-changers, see [52, 53].

²²This is the upper part of the closed curve in Figure 12.

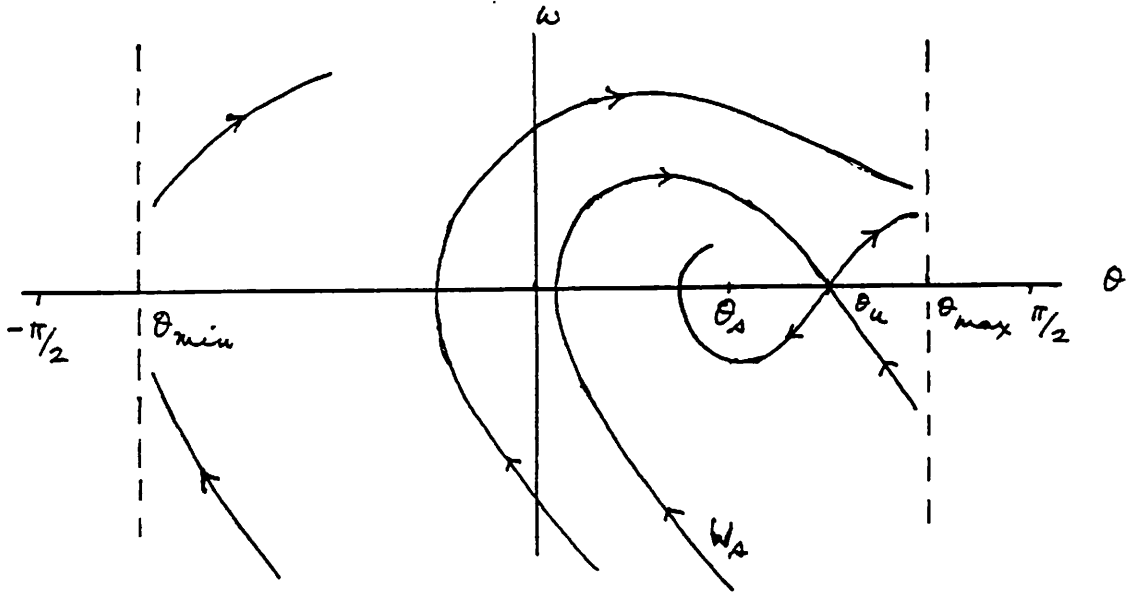


Figure 13: Phase portrait of (25)

We can compare Figure 13 with Figure 5 (where the stable node and saddle are denoted θ and ϕ , respectively). In both cases the transient stability is bounded by the stable manifold W_s of the saddle. In Figure 5, trajectories outside the stability region escape towards the oscillation labeled C . But in Figure 13, trajectories outside the stability region exit the state space at θ_{min} or θ_{max} where the voltage V is at a *minimum*. Thus, *any loss of stability occurs along a trajectory where the voltage will drop suddenly*. We emphasize that this possibility of ‘voltage collapse’ is *not* related to a local bifurcation.²³

Another significant contrast is that θ_s and θ_u in Figure 13 are much closer than θ and ϕ in Figure 5. In fact

$$\theta < \theta_s < \theta_u < \frac{\pi}{2} < \phi$$

Because of this we expect the stability region in Figure 13 to be smaller. Moreover, as Q increases $|\theta_u - \theta_s|$ becomes smaller and the region shrinks further. This effect is nicely demonstrated in the example presented in [54]. At the bifurcation, $\theta_u = \theta_s$, and the phase portrait is as in Figure 14, while beyond the bifurcation, the phase portrait is as in Figure 15. In both instances trajectories exit the state space and there is a ‘voltage collapse’.

The usual explanation of voltage collapse is in terms of Figure 12. One says that when s and u coincide the system has reached its ‘steady state stability limit’. The implication is that the system tracks the stable equilibrium point, s , as the load changes slowly, until $s = u$ beyond which there is no nearby stable equilibrium. However, as we have just seen, the attractor of s also shrinks as s approaches u , and a small disturbance can

²³Of course, θ_{min} and θ_{max} are singularities of (23).

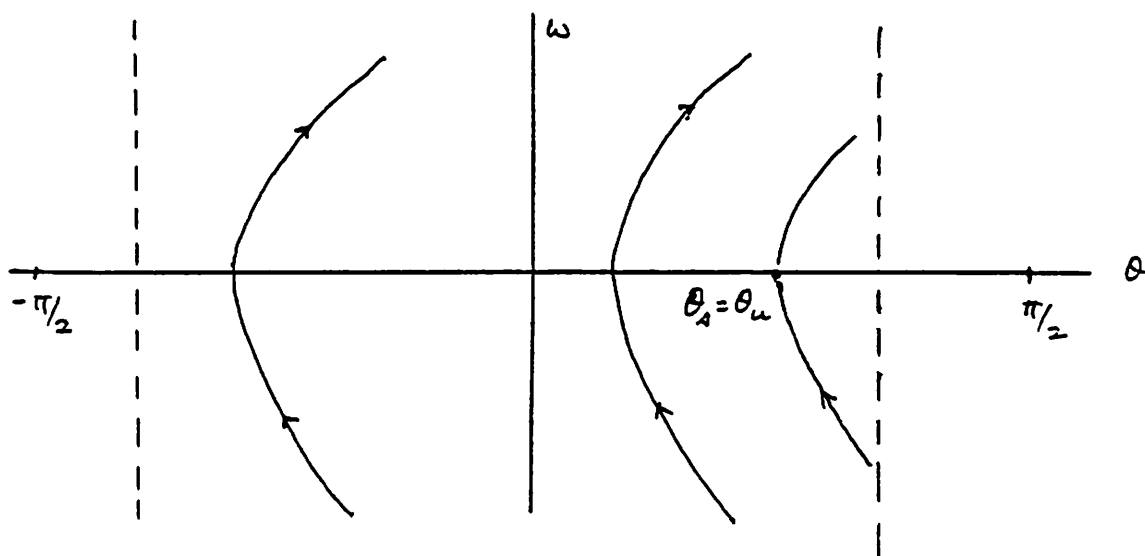


Figure 14: Phase portrait of (25) at bifurcation

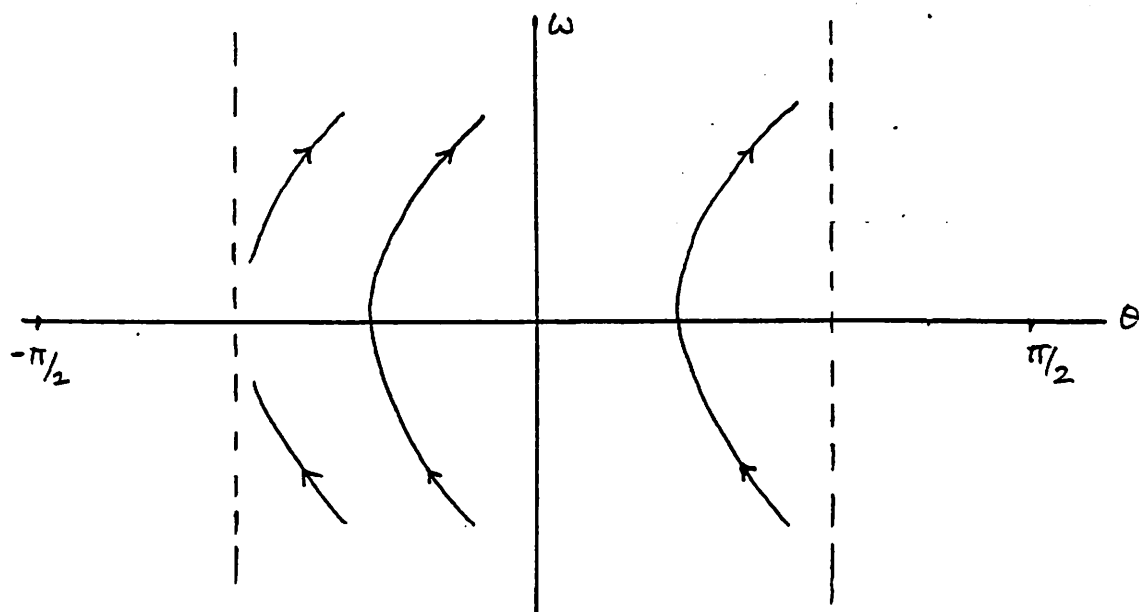


Figure 15: Phase portrait of (25) after bifurcation

then lead to a loss of (transient) stability in a way which causes ‘voltage collapse’. Thus loss of steady state stability and transient instability are complementary rather than competing explanations.

We summarize our discussion of the single generator case.

- The presence of reactive power demand modeled as a PQ bus shrinks the state space since θ_{max} decreases as Q increases.
- The stability region shrinks ($|\theta_u - \theta_s|$ decreases) as either P or Q increases. At the saddle-node bifurcation the stability region vanishes and the system has reached its steady state stability limit.
- Disturbances which move the initial state outside the stability region lead to trajectories along which there is a precipitous drop in voltage. This occurs before bifurcation.
- The onset of bifurcation can be monitored by indices based on the Jacobian of the power flow equation.

2.4.2 The multi-generator case

The power network consists of $n + m + 1$ buses connected by lossless transmission lines and represented by its node admittance matrix $Y = [Y_{ij}] = j[B_{ij}]$. For $i \neq j$, B_{ij} is the susceptance of the line connecting buses i and j . The first n buses are the internal generator buses. Bus $n + 1$ is an infinite bus. These buses are indexed by i or $j = 1, \dots, n + 1$. The m buses indexed l or $k = n + 2, \dots, n + m + 1$ are load buses. The voltages of the first $n + 1$ are $V_i e^{j\theta_i}$; for the infinite bus $V_{n+1} = 1$, $\theta_{n+1} = 0$. The load bus voltages are $V_k e^{j\phi_k}$. The generator buses are PV; the load buses are PQ with demand denoted $P^d + jQ^d$. The mechanical power input is denoted P^m , the electric output power is denoted P^e .

The generator dynamics are modeled by the swing equation

$$\begin{aligned}\dot{\theta}_i &= \omega_i \\ M_i \dot{\omega}_i + D_i \omega_i &= P_i^m - P_i^e\end{aligned}$$

The real and reactive power flow equations at the generator buses $i = 1, \dots, n$ are

$$\begin{aligned}P_i^e &= f_i(\theta, \phi, V) \\ &= \sum_{\substack{j=1 \\ j \neq i}}^{n+1} B_{ij} V_i V_j \sin(\theta_i - \theta_j) + \sum_{k=n+2}^{n+m+1} B_{ik} V_i V_k \sin(\theta_i - \phi_k) \\ 0 &= g_i(\theta, \phi, V) \\ &= -B_{ii} V_i^2 - \sum_{\substack{j=1 \\ j \neq i}}^{n+1} B_{ij} V_i V_j \cos(\theta_i - \theta_j) - \sum_{k=n+2}^{n+m+1} B_{ik} V_i V_k \cos(\theta_i - \phi_k)\end{aligned}$$

At the load buses $k = n + 2, \dots, n + m + 1$ these equations are

$$\begin{aligned} P_k^d &= f_k(\theta, \phi, V) \\ &= \sum_{i=1}^{n+1} B_{ki} V_k V_i \sin(\phi_k - \theta_i) + \sum_{l \neq k}^{n+m+1} B_{kl} V_k V_l \sin(\phi_k - \phi_l) \end{aligned}$$

$$\begin{aligned} Q_k^d &= g_k(\theta, \phi, V) \\ &= -B_{kk} V_k^2 - \sum_{i=1}^{n+1} B_{ki} V_k V_i \cos(\phi_k - \theta_i) - \sum_{l \neq k}^{n+m+1} B_{kl} V_k V_l \cos(\phi_k - \phi_l) \end{aligned}$$

The model is given by

$$\dot{\theta} = \omega \quad (26)$$

$$M\dot{\omega} + D\omega = P^m - f(\theta, \phi, V) \quad (27)$$

$$0 = g_i(\theta, \phi, V), \quad i = 1, \dots, n \quad (28)$$

$$0 = P_k^d - f_k(\theta, \phi, V), \quad k = n + 2, \dots, n + m + 1 \quad (29)$$

$$0 = Q_k^d - g_k(\theta, \phi, V), \quad k = n + 2, \dots, n + m + 1 \quad (30)$$

The state space consists of all $(\omega, \theta, \phi, V) \in R^n \times \Sigma^n$ where Σ^n is the n -dimensional manifold of (θ, ϕ, V) satisfying (28)-(30). As in the single generator case, solutions of this constrained differential equation must be considered with care since they are defined only so long as the state stays within $R^n \times \Sigma^n$. The trajectory can be extended beyond this time by singular perturbations as in [42] or by relaxing the constraints as in [39, 54]. The model is a simplified version of that analyzed in [41].

Let $v_i = \log V_i$ and define the ‘potential’

$$\begin{aligned} V(\theta, \phi, v; P^d, Q^d) &:= -\langle P^m, \theta \rangle - \langle P^d, \phi \rangle - \langle Q^d, v \rangle \\ &- \sum_{i=1}^n \frac{1}{2} B_{ii} e^{2v_i} - \sum_{i < j} B_{ij} e^{v_i + v_j} \cos(\theta_i - \theta_j) \\ &- \sum_{i=1}^n \sum_{k=n+2}^{n+m+1} B_{ik} e^{v_i + v_k} \cos(\theta_i - \phi_k) \\ &- \sum_{k < l}^{n+m+1} B_{kl} e^{v_k + v_l} \cos(\phi_k - \phi_l) - \sum_{k=n+2}^{n+m+1} \frac{1}{2} B_{kk} e^{2v_k} \end{aligned}$$

Then (26)-(30) can respectively be reexpressed as

$$\begin{aligned} \dot{\theta} &= \omega \\ M_i \dot{\omega} + D_i \omega_i &= -\frac{\partial V}{\partial \theta_i}, \quad i = 1, \dots, n \\ 0 &= -\frac{\partial V}{\partial v_i}, \quad i = 1, \dots, n \end{aligned}$$

$$0 = -\frac{\partial V}{\partial \phi_k}, \quad k = n + 2, \dots, n + m + 1$$

$$0 = -\frac{\partial V}{\partial v_k}, \quad k = n + 2, \dots, n + m + 1$$

The state $(\omega = 0, \theta, \phi, v)$ is an equilibrium if the gradient of V vanishes at (θ, ϕ, v) . Define the energy function of the state,

$$W(\omega, \theta, \phi, v) := \frac{1}{2} \sum_i M_i \omega_i^2 + V(\theta, \phi, v)$$

The energy function²⁴ serves as a Lyapunov function since along trajectories

$$\frac{dW}{dt} = - \sum D_i \omega_i^2$$

Thus equilibrium points coincide with the critical points of the potential function and local bifurcations of the equilibrium will coincide with catastrophes of the potential function. The typical bifurcation is a fold catastrophe. It can be shown that a stable equilibrium point is likely to bifurcate as a saddle-node bifurcation [55, 33, 56, 57].

In contrast to the single generator case where a fairly complete analysis was possible, there are no quantitative results for the general case. Claims that the bifurcation leads to ‘voltage collapse’ are all based on simple examples [41, 56, 58]. One interesting result of [38], similar to that of Fact 2.3, provides some insight.

Fact 2.4 Suppose the network has no direct load to load connection, i.e. $B_{kl} = 0$ for $k \neq l$. An equilibrium (θ, ϕ, V) is stable if

1. $|\theta_i - \theta_j| < \pi/2$ whenever $B_{ij} > 0$
2. $\cos(\theta_i - \phi_k) > V_i/2V_k$ whenever $B_{ik} > 0$

Observe that condition 1 is the same as (18) and seems likely to hold at operating points. On the other hand condition 2 becomes increasingly restrictive as the load bus voltage drops (V_k decreases) which is likely to occur as reactive power demand increases. *Thus we conjecture that in general increases in reactive power demand reduce the stability region.* Assuming the conjecture is true, we still need to know whether unstable trajectories exhibit precipitous voltage decline. We summarize one final result along these lines.

Suppose the instability occurs at a saddle-node bifurcation. This is a critical point of the potential V , and so the Hessian of V has one zero eigenvalue. Then the resulting trajectory is likely to be close to the so-called ‘center manifold’ at the equilibrium, see [2]. The tangent to the center manifold at the equilibrium is the eigenvector associated with

²⁴This particular treatment is adapted from [38]. W is one of a family of ‘structure-preserving’ energy functions, see also [39, 40].

the zero eigenvalue of the Hessian at V . One can then numerically integrate the trajectory in the direction of the eigenvector to see if there is a voltage collapse along it. Simple examples suggest that this is the case [56].²⁵ Reference [56] provides a complete account of the argument that voltage collapse results from a saddle-node bifurcation. The account also subsumes several other explanations based on ‘static’ sensitivity indices.

Lastly, we must note that as in §2.3.2, there are in all likelihood global bifurcations which create oscillatory instabilities. However, there are no results along these directions.

2.4.3 Practical implications

As the EPRI Proceedings on voltage stability and security from which an earlier paper [47] was quoted suggest, voltage instability is a serious problem. Its causes are yet unclear although there is some evidence and greater agreement that it is caused by the inability to meet reactive power demand. The analytical studies summarized above shed some light on this problem.

- The study of the single generator system shows that increases in reactive power demand must increase the chances of instability and unstable trajectories must exhibit voltage collapse. This can occur well before bifurcation. Strengthening the transmission capacity (reducing B) increases stability.
- In the general case, useful analytical results are scarce and are at best only suggestive of the strong conclusions based on the single generator case. It is likely that additional modes of instability due to global bifurcations are present, although this is conjectural. More serious analytical and numerical studies must be undertaken before one can be confident about these conclusions.

²⁵In the example studied in [56], it is noted that the voltage component of the eigenvector has a negative sign and it is concluded from this that “the voltage will decrease at the bifurcation, at least initially.” However, this conclusion is incorrect since the negative of the eigenvector (which would have a positive voltage component) is also an eigenvector.

3 Hopf bifurcation

Until now we were mostly concerned with bifurcations of

$$\dot{x}(t) = f(x(t), \gamma)$$

arising from a change in the number of equilibria. This is a local bifurcation since it is signaled by the local condition

$$f(x_0, \gamma_0) = 0, \quad \det \frac{\partial f}{\partial x}(x_0, \gamma_0) = 0$$

The Hopf bifurcation is also a local bifurcation of an equilibrium in that its occurrence is determined by the local behavior of f . However, it requires an analysis of higher order derivatives of f at (x_0, γ_0) . We first explain the Hopf bifurcation and then examine its occurrence in power systems.

3.1 The Hopf bifurcation theorem

The following discussion is adapted from [2, 59, 60, 61, 62]. Consider the two-dimensional linear system

$$\begin{aligned}\dot{x}_1 &= \gamma x_1 - \omega x_2 \\ \dot{x}_2 &= \omega x_1 + \gamma x_2\end{aligned}$$

When $\gamma < 0$ all trajectories spiral into the equilibrium at 0; when $\gamma = 0$ all trajectories are periodic; and when $\gamma > 0$ all trajectories spiral out from 0. Since the resulting phase portraits are not topologically orbital equivalent (see §2.1) there is a bifurcation at $\gamma = 0$. The phase portrait at 0 consisting of a whole family of periodic orbits is rather special and unlikely to persist if the differential equation is perturbed by a nonlinearity. It turns out, however, that there will be a periodic orbit in the more general case.

Any parameterized two-dimensional system with an equilibrium at 0 can be cast by a smooth change of coordinates into the polar form

$$\begin{aligned}\dot{r} &= (d\gamma + ar^2)r \\ \dot{\theta} &= \omega + c\gamma + br^2\end{aligned}$$

The origin is an equilibrium. If $d \neq 0$, there is a bifurcation at $\gamma = 0$ since the origin is stable for $d\gamma < 0$ and unstable for $d\gamma > 0$. Since the first equation does not depend on θ , we see immediately that there are periodic orbits, $r = \text{constant}$. If $a \neq 0$ and $d \neq 0$ these solutions lie along the parabola $d\gamma + ar^2 = 0$. The Hopf bifurcation theorem says that this situation holds in general.

The theorem describes the emergence of a periodic solution from an equilibrium $x_0(\gamma)$ of the equation

$$\dot{x} = f(x, \gamma) \tag{31}$$

where $x \in R^n$ and $\gamma \in R$ is a real parameter. Existence of a family of bifurcating periodic solutions is assured (under some additional technical conditions) if the linearization of (31) possesses a pair of complex conjugate eigenvalues which cross the imaginary axis as γ passes through a critical value γ_0 . The theorem also gives information on the range of parameter values for which the periodic solutions arise, their amplitude, frequency and stability. The following hypotheses are in force throughout.

1. System (31) has an isolated equilibrium at $x_0(\gamma)$.
2. $f(x, \gamma)$ is C^r ($r \geq 4$).
3. The Jacobian $\partial f(x_0(\gamma), \gamma)/\partial x$ possesses a pair of complex conjugate, simple eigenvalues

$$\lambda(\gamma) = \alpha(\gamma) + j\omega(\gamma), \quad \bar{\lambda}(\gamma) = \alpha(\gamma) - j\omega(\gamma)$$

4. At the critical value

$$\alpha(\gamma_0) = 0, \quad \omega_0 := \omega(\gamma_0) > 0, \quad \text{and} \quad \alpha'(\gamma_0) > 0$$

Besides $\pm j\omega_0$, the other eigenvalues of the critical Jacobian $\partial f(x(\gamma_0), \gamma_0)/\partial x$ have strictly negative real part.

For definiteness, we have required $\alpha'(\gamma_0) > 0$, although $\alpha'(\gamma_0) \neq 0$ is sufficient. This so-called *Hopf condition* means that the eigenvalues $\lambda(\gamma)$, $\bar{\lambda}(\gamma)$ cross the imaginary axis into the right half plane transversally at γ_0 .²⁶ Bifurcation to periodic solutions will also occur if some of the eigenvalues of the critical Jacobian have positive real part, but the resulting oscillations will be unstable.

Linearized analysis of (31) suggests the presence of small-amplitude oscillations for γ near γ_0 . The theorem below (adapted from [61]) asserts this is indeed the case.

Theorem (The Hopf bifurcation theorem)

Existence. There is $\epsilon_H > 0$ and a C^{r-1} function

$$\gamma(\epsilon) = \gamma_0 + \gamma_2 \epsilon^2 + O(\epsilon^3)$$

and for each $0 < \epsilon < \epsilon_H$ there is a nonconstant periodic solution $x_\epsilon(t)$ of (31) near the equilibrium $x_0(\gamma)$ for the parameter value $\gamma = \gamma(\epsilon)$. The period of x_ϵ is a C^{r-1} function

$$T(\epsilon) = 2\pi\omega_0^{-1}[1 + T_2\epsilon^2] + O(\epsilon^3)$$

and its amplitude grows as $O(\epsilon)$.

Uniqueness. If $\gamma_2 \neq 0$ then there is $\epsilon_0 > 0$ such that for each $0 < \epsilon < \epsilon_0$, x_ϵ is the only periodic orbit for $\gamma = \gamma(\epsilon)$ near $x_0(\gamma(\epsilon))$.

Stability. Exactly one of the characteristic exponents of $x_\epsilon(t)$ approaches 0 as $\epsilon \rightarrow 0$, and it is given by the real C^{r-1} function

$$\beta(\epsilon) = \beta_2 \epsilon^2 + O(\epsilon^3)$$

²⁶If $\alpha'(\gamma_0) = 0$, the *degenerate* Hopf bifurcation results, see §3.3.

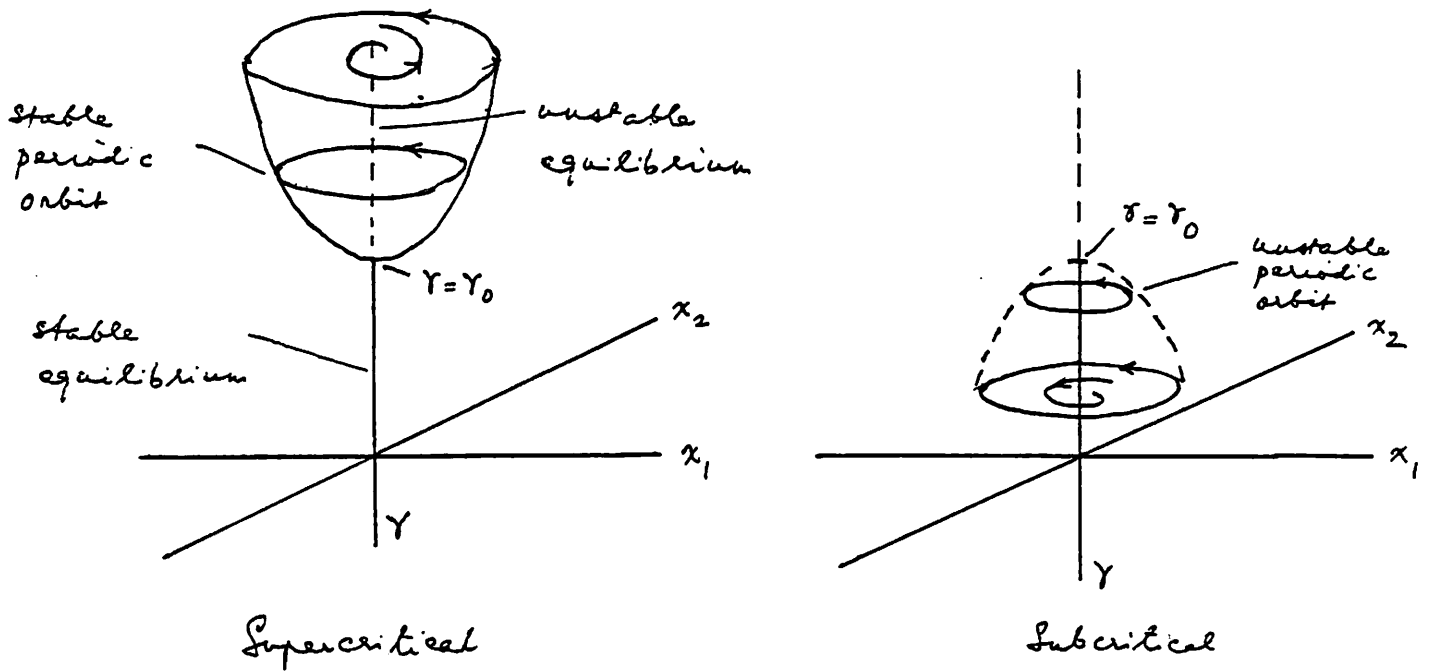


Figure 16: The Hopf bifurcation

The relationship

$$\beta_2 = -2\alpha'(\gamma_0)\epsilon_2 \quad (32)$$

holds. Moreover the periodic solution $x_\epsilon(t)$ is orbitally asymptotically stable with asymptotic phase if $\beta(\epsilon) < 0$ but is unstable if $\beta(\epsilon) > 0$.²⁷

For a linear system satisfying the hypotheses above, a little reflection shows that the predicted family of periodic solutions occurs only for $\gamma = \gamma_0$, so that $\gamma(\epsilon) \equiv \gamma_0$. Hence γ_2, T_2 and β_2 must all vanish in the linear case. If $\gamma_2 \neq 0$, then the periodic solutions $x_\epsilon(t)$ occur either for $\gamma > \gamma_0$ or for $\gamma < \gamma_0$. The bifurcation is said to be *supercritical* in the former case and *subcritical* in the latter. If γ_2, β_2 are both nonzero, then the direction of bifurcation, i.e. $\gamma > \gamma_0$ or $\gamma < \gamma_0$, and the stability of oscillations are determined by the coefficients γ_2 and β_2 respectively. In light of (32), the oscillations are stable, respectively unstable, if they are supercritical, respectively subcritical. For this reason, (32) is called Hopf's *exchange of stability formula*. Figure 16 shows the two possibilities for a two-dimensional system with an equilibrium at the origin. Note that the amplitude of the oscillation grows as $|\gamma - \gamma_0|^{1/2}$.

If the four hypotheses hold, which is easy to check, it is certain that there is a Hopf bifurcation to periodic solutions at γ_0 . Determining the stability of the bifurcation requires evaluating β_2 and that takes more effort. In [61] explicit 'bifurcation formulas' are obtained for ϵ_2, T_2 and β_2 . There are two cases.

Case 1. Suppose $n = 2$ and that (31) has been transformed into 'standard canonical form.'

²⁷For definitions of characteristic exponent and orbital stability see [63].

This means $x_0(\gamma) \equiv 0$ and

$$\frac{\partial f}{\partial x}(0, \gamma) = \begin{bmatrix} \alpha(\gamma) & \omega(\gamma) \\ -\omega(\gamma) & \alpha(\gamma) \end{bmatrix}$$

Recall that $\alpha(\gamma_0) = 0$ and $\omega_0 = \omega(\gamma_0) > 0$. Then β_2 is given by the formula

$$\begin{aligned} 8\beta_2 &= \frac{1}{\omega_0} \{ f_{11}^1(f_{11}^2 - f_{12}^1) + f_{22}^2(f_{12}^2 - f_{22}^1) + (f_{11}^2 f_{12}^2 - f_{12}^1 f_{22}^1) \} \\ &+ (f_{111}^1 + f_{122}^1 + f_{112}^1 + f_{222}^1) \end{aligned}$$

Here

$$f = (f^1, f^2), \quad f_{pq}^i = \frac{\partial^2 f^i}{\partial x_p \partial x_q}(0, \gamma_0), \quad f_{pqr}^i = \frac{\partial^3 f^i}{\partial x_p \partial x_q \partial x_r}(0, \gamma_0)$$

Case 2. In the general case, one uses the center manifold theorem to reduce the n -dimensional system (31) satisfying the hypotheses to a two-dimensional ‘essential model’ of Case 1 for the study of the bifurcated periodic solutions.

The algorithm in [61] for computing γ_2, T_2 and β_2 for general n -dimensional systems has been programmed by B. Hassard.²⁸ That program, BIFOR2, has been used in several studies to evaluate Hopf bifurcation in power systems. We review these next.

3.2 Hopf bifurcation due to excitation control

We summarize the investigations of Hopf bifurcation in power systems due to the effect of excitation control. The effect of excitation system parameters on power system stability has been studied for a long time [64, 65]. In [66] it was observed that the stability of a power system was sensitive to changes in the amplifier gain K_A of the exciter. Oscillations were observed to take place, but no rigorous analysis was given. The phenomenon was correctly examined in [62, 67] within the framework of Hopf bifurcation theory.

Consider a synchronous machine connected to an infinite bus with fixed voltage Ee^{j0} . If the transmission line has impedance $R_l + jX_l$, and amortisseur effects, armature resistance, armature $\dot{\psi}$ terms and saturation are neglected, one gets the model [37]

$$\begin{aligned} V_t^2 &= v_d^2 + v_q^2 \\ -v_d &= \psi_q = -X_q i_q \\ v_q &= \psi_d + E'_q + (X_q - X'_d) i_d \\ P_e &= E_q i_q \\ i_d &= x(E_q - E \cos \theta) - rE \sin \theta \\ i_q &= r(E_q - E \cos \theta) + xE \sin \theta \\ \tau' \dot{E}'_q &= E_{FD} - E'_q - (X_d - X'_d) i_d \\ 2H\ddot{\theta} + D\dot{\theta} &= \omega_0(P_m - P_e) \end{aligned}$$

²⁸ A detailed discussion along with the program listing can be found in [61].

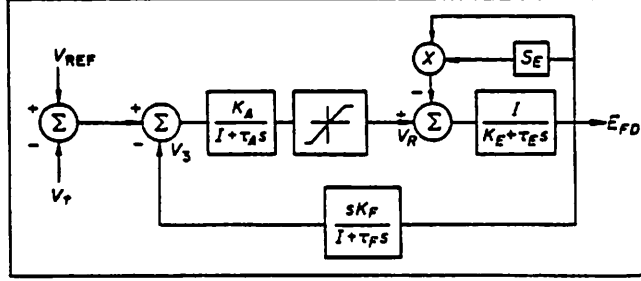


Figure 17: IEEE Type 1 excitation system

where

$$x = \frac{X_l + X_q}{R_l^2 + (X_l + X_q)^2}, \quad r = \frac{R_l}{R_l^2 + (X_l + X_q)^2}$$

The notation used here is standard [37] and will not be elaborated further; ω_0 is the frequency of the voltage at the infinite bus, d and q refer to the direct and quadrature axes. This model describes machine behavior provided it is not equipped with an excitation control system, i.e. if the field voltage E_{FD} is constant. Suppose there is a continuously acting excitation system. Then E_{FD} will be governed by the excitation system dynamics. The IEEE Type 1 excitation system has the machine terminal voltage V_t as input and its output is E_{FD} , see Figure 17. If the limiter is neglected, it can be modeled by the equations

$$\begin{aligned} \tau_E \dot{E}_{FD} &= -K_E E_{FD} + V_R - E_{FD} S_E(E_{FD}) \\ \tau_F \dot{V}_3 &= -V_3 + \frac{K_F}{\tau_E} (-K_E E_{FD} + V_R - E_{FD} S_E(E_{FD})) \\ \tau_A \dot{V}_R &= -V_R + K_A (V_{REF} - V_t - V_3) \end{aligned}$$

The saturation function is approximated as

$$S_E(E_{FD}) = A_{EX} \exp(B_{EX} E_{FD})$$

where the coefficients A_{EX} and B_{EX} are computed from saturation data.

The occurrence of oscillations was investigated for the following model parameter values.

Machine	Exciter	Transmission line
$H = 2.37s$	$K_E = -0.05$	$R_l^0 = 0.02$
$D = 1 \text{ p.u.}$	$K_F = 0.02$	$X_l^0 = 0.40$
$X_d = 1.7$	$\tau_E = 0.50s$	$R_l = \lambda R_l^0$
$X_q = 1.64$	$\tau_A = 0.10s$	$X_l = \lambda X_l^0$
$\omega_0 = 377 \text{ rad/s}$	$A_{EX} = 0.09$	
$\tau'_{d0} = 5.9s$	$B_{EX} = 0.50$	

The bifurcation parameter is $\gamma = K_A^{1/2}$ to ensure that $K_A > 0$. The program BIFOR2 searches for a critical value γ_0 and an equilibrium point of the model for which the hypotheses of the Theorem are satisfied. Several cases are studied numerically to permit some general conclusions to be drawn. Each case is determined by specifying an initial guess for an equilibrium (required by the program) and a parameter λ which has the effect of changing the length of the transmission line

$$R_l + jX_l = \lambda[R_l^0 + jX_l^0]$$

where R_l^0, X_l^0 are nominal parameters. Four sets of results are given in [62, 67] to show the qualitatively distinct possibilities that may arise. The first two cases correspond to generator action ($P_m > 0$), the others to motor action ($P_m < 0$). Examples with $\beta_2 > 0$ and $\beta_2 < 0$ are given in each case. Only the generator case is reproduced below. An equilibrium point of the sixth order model above is denoted by

$$x_0 = (\theta^0, \omega^0, E_q^0, E_{FD}^0, V_3^0, V_R^0)$$

Example 1. ($P_m > 0, \beta_2 > 0$) Here $P_m = 0.937, V_{REF} = 1.13, \lambda = 2$. The equilibrium is

$$x_0 = (1.351, 0, 1.105, 2.316, 0, 0.548)$$

BIFOR2 computes the values

$$\omega_0 = 7.569, \gamma_2 = -4.71, T_2 = 0.164, \beta_2 = 0.359$$

$$\gamma_0 = 13.919 (K_A = 193.7), \alpha'(\gamma_0) = 0.038$$

using the notation of the Theorem. By the Theorem, a bifurcation to periodic orbits occurs at the critical value $K_A = 193.7$, and there is a locally unique unstable periodic solution in the vicinity of x_0 for $K_A < 193.7$ and $(193.7 - K_A)$ sufficiently small. Thus this is the subcritical case.

Example 2. ($P_m > 0, \beta_2 < 0$) Now $P_m = 2.272, V_{REF} = 1.244, \lambda = 0.8$. The equilibrium is

$$x_0 = (1.363, 0, 1.42, 4.53, 0, 3.69)$$

BIFOR2 computes the values

$$\omega_0 = 11.47, \gamma_2 = 2.61, T_2 = 0.129, \beta_2 = -0.206$$

$$\gamma_0 = 18.975 (K_A = 360.1), \alpha'(\gamma_0) = 0.039$$

By the Theorem, there is a bifurcation to a stable periodic solution for sufficiently small $K_A > 360.1$. This is the supercritical case.

Two general conclusions may be offered from these examples.

- The angle difference θ_0 between the generator terminal and infinite bus voltages at bifurcation is quite large (~ 60 deg). This corresponds to large real power flow. A similar behavior was reported in [66], where it was noted that the oscillatory instability disappeared when the input power (and hence θ_0) was reduced.

- It would seem that the subcritical case, Example 1, is more likely to be seen in practice. This conclusion is confirmed by a recent study involving two generators supplying a PQ load, and the real power demand is taken as the bifurcation parameter, [68]. In the subcritical case the equilibrium is stable but is surrounded by an unstable limit cycle. Hence the stability region is reduced.

Simulations of a reduced third order model are also reported in [67].²⁹ The simulations confirm estimates provided by the Theorem: the period of oscillation is close to that given by the critical imaginary eigenvalue, $T \sim (2\pi)\omega_0^{-1}$; and the amplitude of the oscillation grows as K_A moves away from its critical value. The generator terminal voltage swings by as much as 10% p.u. so that the instability is severe.

Also reported in [67] is an interesting attempt at constructing the global dynamics of the reduced order model in the subcritical case. It is shown that the stability region of the equilibrium is bounded by the unstable periodic orbit (see Figure 16). The amplitude of the orbit, and hence the the stability region, grows as K_A moves away from its critical value, until the orbit hits the saddle point (see the saddle ϕ in Figure 4). At this point a global bifurcation occurs, the periodic orbit disappears, and the stability region resembles that in Figure 5.

In the studies reviewed so far the Hopf condition $\alpha'(\gamma_0) > 0$ holds so the pair of complex eigenvalues $\alpha(\gamma) \pm j\omega(\gamma)$ cross the imaginary axis into the right half plane transversally at $\gamma = \gamma_0$. The Hopf bifurcation theorem then applies and the occurrence of oscillatory instability follows immediately.

It is possible that this pair of complex eigenvalues recrosses the imaginary axis into the left half plane at another value $\gamma = \gamma_1$ where $|\gamma_0 - \gamma_1|$ is small. In this case the practical conclusions based on the Theorem concerning the nature of the instability and the size of the periodic orbits only hold in a very small region of parameter values near γ_0 . Together with the fact the model is only an approximation, this leads to the realization that those conclusions are not robust. In such a case it is essential to understand what happens in the *degenerate* case, $\alpha'(\gamma_0) = 0$.

The study of the degenerate case is much more delicate for two reasons. First, there can be many qualitatively different types of bifurcating behavior [70], in contrast with the two types of supercritical and subcritical bifurcations in the non-degenerate case. Second, the analytical and numerical studies needed to determine which type of bifurcation occurs are much more difficult.

Such a study is conducted in [71] for essentially the same model as that considered above, but involving two generators and an infinite bus connected by lossy transmission lines. The analysis involves the use of the Lyapunov-Schmidt procedure used in [14, 41], except that it is now infinite-dimensional [72]. When the procedure can be carried out, it yields a reduced order model which exhibits the essential bifurcation behavior. In that case explicit formulas, similar but involving higher order derivatives than those presented under

²⁹The reduced order model is justified by a time-scale separation based on singular perturbation theory. A general treatment of singularly perturbed Hopf bifurcation appears in [69].

Case 1 in §3.1, are available [70]. For the ninth-order model considered in [71] this approach is not feasible, and a numerical study was carried out to determine the type of bifurcation. The numerical study yields a (local) bifurcation diagram which is then compared with the ‘universal unfolding normal forms’ of [70] and classified accordingly. The details are too complex to be presented here. However, the study suggests one conclusion.

- Complicated degenerate Hopf bifurcations can certainly occur. Although these cannot be studied by analytical techniques alone because of the high dimension of the systems involved, analysis combined with very careful numerical study can lead to an understanding of the bifurcation behavior.

3.3 Other Hopf bifurcations

The only other study seems to be [62] which reports three additional examples of Hopf bifurcation. Two of these consider more accurate versions of the swing equation for a single machine connected to an infinite bus,

$$M\ddot{\theta} + D\dot{\theta} = P - B \sin \theta + G \cos \theta$$

In the first example, the damping is taken to be a function of the state,

$$D(\theta) = [a \sin^2 \theta + b \cos^2 \theta] - r[c(1 - \tan^2 \theta) + d(1 - \sin 2\theta)]$$

This model is from [73], see also [74]. This second order model is transformed into the standard canonical form of Case 1 in §3.1. It is then shown that for some parameter values the negative damping leads to a Hopf bifurcation.

The second example refines the model to take into account the fact that the delivered electrical power,

$$P_e = B \sin \theta + G(1 - \cos \theta)$$

is related to the electrical torque by

$$P_e = (\omega_0 + \dot{\theta})T_e$$

where ω_0 is the synchronous frequency and $\dot{\theta}$ is the instantaneous frequency deviation. Again this is a second order model and can be studied by analytical means. It is shown that Hopf bifurcation can arise as P is varied.

The third example involves interaction between the swing equation and the electrical transmission lines. Two generators connected by a lossy transmission are considered,

$$\begin{aligned} \ddot{\theta}_1 + D_1\dot{\theta}_1 &= \omega_0[P_1 - B \sin(\theta_1 - \theta_2) + G(\cos(\theta_1 - \theta_2))] \\ \ddot{\theta}_2 + D_2\dot{\theta}_2 &= \omega_0[P_2 + B \sin(\theta_1 - \theta_2) + G(\cos(\theta_1 - \theta_2))] \end{aligned}$$

This fourth order system is reduced to a third order system which is studied numerically. It is shown that a subcritical Hopf bifurcation can occur using G as the bifurcation parameter.

From all these studies it is clear that when the swing equation is combined with other dynamics that can compensate for its (nominal) negative damping, a Hopf bifurcation can occur.

3.4 Practical implications

There are very few studies of Hopf bifurcation, perhaps because this possibility was noted relatively recently, and perhaps because such studies require a judicious combination of analysis and careful numerical study. Even those few studies, however, support the following conclusions.

- Hopf bifurcations can occur due to the interaction of the swing equations with other parts of the electrical system (exciter system, transmission lines).
- The typical case is that of a subcritical bifurcation in which the operating point is stable, but its region of (transient) stability is reduced by the surrounding unstable periodic orbit. As the loading is reduced, the unstable orbit grows, the region of stability increases. The orbit probably disappears in a global bifurcation as it 'hits' a saddle equilibrium. This is conjectural.
- The bifurcation can be degenerate and qualitatively new types of behavior can appear.

4 Chaos

We begin with a brief review of the essential concepts of chaos theory. We then review the literature on chaos in power systems.

4.1 Basic concepts

4.1.1 Poincaré map

The material here is largely adapted from [5, 9]. Consider the system

$$\dot{x} = f(x) + \gamma g(x, t) \quad (33)$$

where $x \in R^n$, $\gamma \in R$ is a small parameter, and $g(x, t)$ is periodic in t with period T . We will think about (33) as the time-invariant system

$$\dot{x} = f(x)$$

forced by a (state-dependent) periodic input. We can convert (33) into the time-invariant system

$$\begin{aligned} \dot{x} &= f(x) + \gamma g(x, \delta) \\ \dot{\delta} &= 1 \end{aligned} \quad (34)$$

The state $(x, \delta) \in R^n \times \Sigma$ where $\Sigma = [0, T]$ and δ is measured modulo T . The dimension of this system is increased to $n + 1$.³⁰

Let $(x(t), \delta(t)) = \Phi(t; x_0, \delta_0) \in R^n \times \Sigma$ be the trajectory of (34) at time t starting in the initial state (x_0, δ_0) at time 0. Let $x_n = x(nT)$, $\delta_n = \delta(nT)$, $n = 0, \pm 1, \pm 2, \dots$ be the samples of this trajectory spaced T apart. Then

$$(x_{n+1}, \delta_{n+1}) = \Phi(T; x_n, \delta_n) \quad (35)$$

Moreover, since $\delta_n \equiv \delta_0$, (35) defines a discrete time system in x_n alone,

$$x_{n+1} = F(x_n; \gamma, \delta_0) \quad (36)$$

Thus we have reduced the state space dimension by 1. In (36) the dependence of F on γ and δ_0 is explicitly noted; however, since δ_0 will remain fixed throughout, we will drop that argument.

Note that if $\hat{x}(t)$ denotes the trajectory of (33) starting in state x_0 at time δ_0 , then for all n

$$x_n = \hat{x}(nT + \delta_0)$$

so (36) is just the sampled version of (33). The map F is called the *Poincaré map*, see Figure 18.

³⁰(34) is called the *suspended system*.

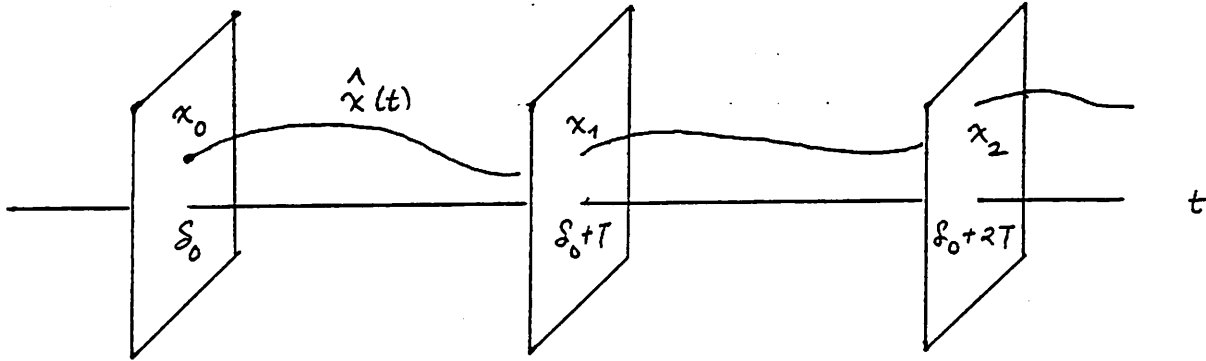


Figure 18: The Poincaré map

4.1.2 The homoclinic tangle

Suppose $n = 2$, and consider the unforced system ($\gamma = 0$),

$$\dot{x} = f(x) \quad (37)$$

Suppose (37) has a saddle point equilibrium p such that one branch of its stable manifold coincides with one branch of its unstable manifold as shown in Figure 19 b. More generally, we may have two saddles, p and q , and a cycle of orbits as in Figure 19 a. If $p \neq q$, these are *heteroclinic orbits*; if $p = q$ these are *homoclinic orbits*. We only discuss the homoclinic case since it arises in power system models. However, the argument for the heteroclinic case is similar.

Now consider the Poincaré map of (37),

$$x_{n+1} = F(x_n; \gamma = 0) \quad (38)$$

p will again be a saddle point of F . The unstable and stable manifolds of p will also be the same as before, where

$$\begin{aligned} W_s(p) &= \{x_0 \mid F^n(x_0) \rightarrow p \text{ as } n \rightarrow \infty\} \\ W_u(p) &= \{x_0 \mid F^{-n}(x_0) \rightarrow p \text{ as } n \rightarrow \infty\} \end{aligned}$$

See Figure 20. Of course the closed curve in Figure 20 is no longer a single orbit of (38) (as it was in the case of (37)), since orbits of (38) consists of a sequence of points

$$x_n = F^n(x_0), \quad n = 0, \pm 1, \pm 2, \dots$$

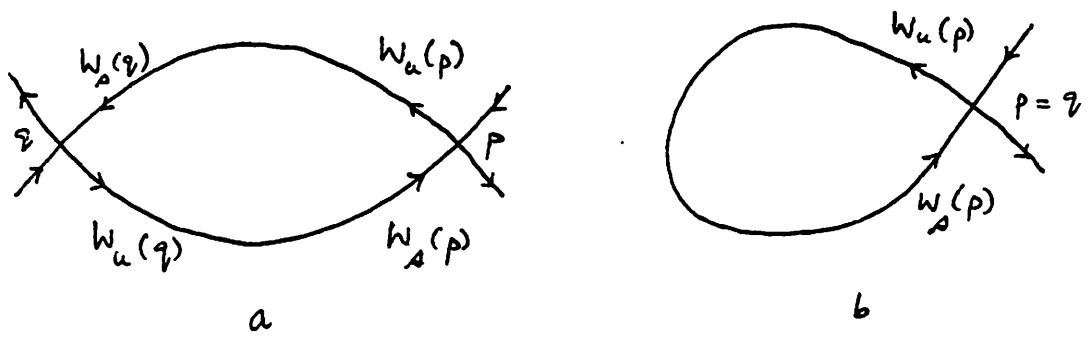


Figure 19: Heteroclinic and homoclinic saddle connections

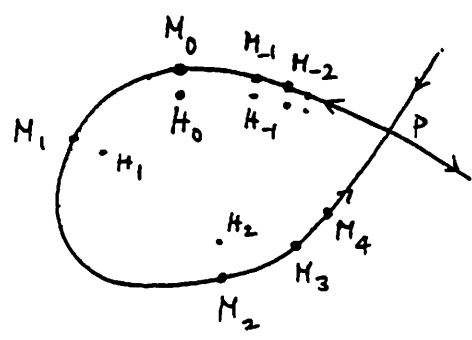


Figure 20: Orbits of (38)

Parts of two orbits $\{\dots M_{-2}, M_{-1}, M_0, M_1, \dots\}$ and $\{\dots H_{-1}, H_0, H_1, \dots\}$ are shown in Figure 20.

We now introduce the periodic forcing term, $\gamma \neq 0$, γ small. If we want to study the behavior of (33) directly we must display the phase portrait of the three dimensional system (34). This is rather difficult. But we can gain a lot of information from the orbit structure of the *two* dimensional discrete time system (36), namely

$$x_{n+1} = F(x_n, \gamma) \quad (39)$$

We will study this orbit structure.

First, note that $F(p, 0) = p$, since p is an equilibrium of the unforced system. If $\gamma \neq 0$ is small enough, by the Implicit Function Theorem there will be a saddle p_γ for the forced system (39),

$$F(p_\gamma, \gamma) = p_\gamma$$

(In the continuous time system (33) there is a periodic orbit through p_γ of period T , see [2] or [9], which collapses to an equilibrium of the sampled system (39).)

Second, and more important, the stable and unstable manifolds of p_γ , $W_s(p_\gamma)$ and $W_u(p_\gamma)$, may no longer coincide.³¹

The breakup of the homoclinic orbit results in one of two cases. Either the two manifolds will no longer intersect as in Figure 21 a; or they will intersect transversally at the point q as in Figure 21 b.³² In the figure we have dropped the subscript γ from p . The point q is called a *homoclinic* point, or q is said to be homoclinic to p . Suppose henceforth that the introduction of the forcing term leads to a transversal intersection as in Figure 21 b. This is a structurally stable situation since, by the Implicit Function Theorem again, small changes in γ will preserve the intersection although the point q will move as γ changes. But we will see now that the intersection implies a radical alteration in the orbit structure from that of Figure 21 b. We attempt to arrive at a true depiction of this structure in a sequence of corrections to Figure 21 b. The discussion below follows [4].

Correction 1. Since $q \in W_s$, its positive iterates

$$q_1 = F(q; \gamma), q_2 = F^2(q; \gamma), \dots$$

converge to p along W_s . Its negative iterates

$$q_{-1} = F^{-1}(q; \gamma), q_{-2} = F^{-2}(q; \gamma), \dots$$

converge to p along W_u . But the *negative* iterates of q_1, q_2, \dots must converge to p also, and so they belong to W_u as well; and the *positive* iterates of q_{-1}, q_{-2}, \dots must converge to p , and so they belong to W_s as well. Thus W_s and W_u *must intersect not only at q but also at $q_{\pm 1}, q_{\pm 2}, \dots$* . Thus we obtain an infinite sequence of homoclinic points and our first correction as in Figure 22.

³¹The coincidence of these manifolds in Figure 20 is an exceptional, or structurally unstable, occurrence. This is easy to see: since both manifolds are one dimensional, a small appropriate change in F will cause them to move apart.

³²Transversal intersection means that the tangents to the two manifolds at q span the state space.

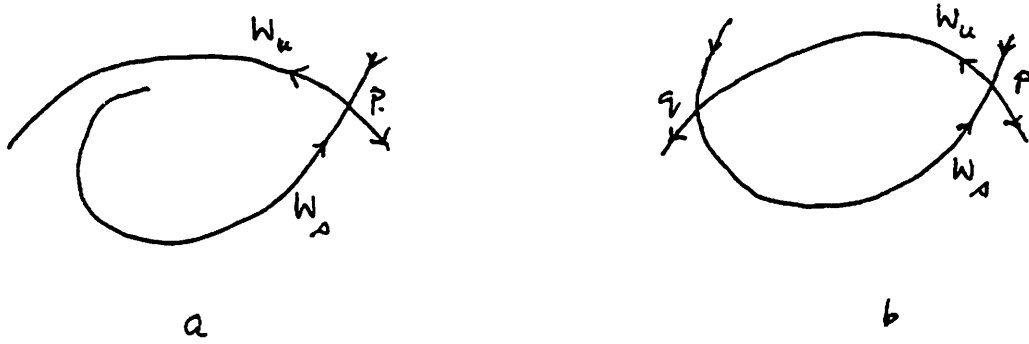


Figure 21: Breakup of homoclinic orbit

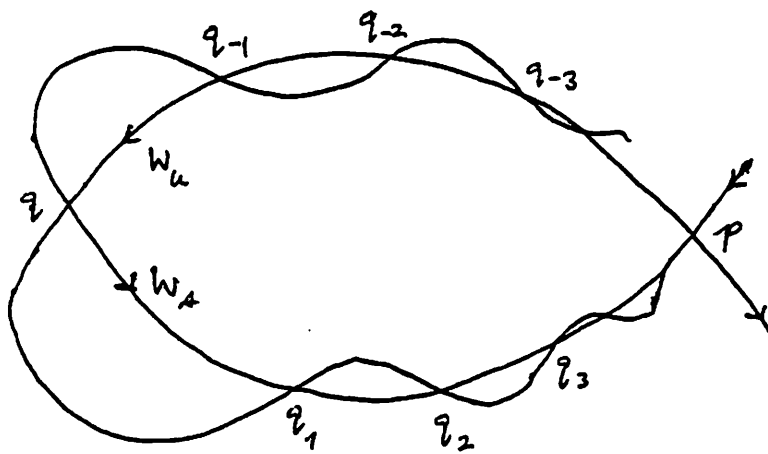


Figure 22: First correction

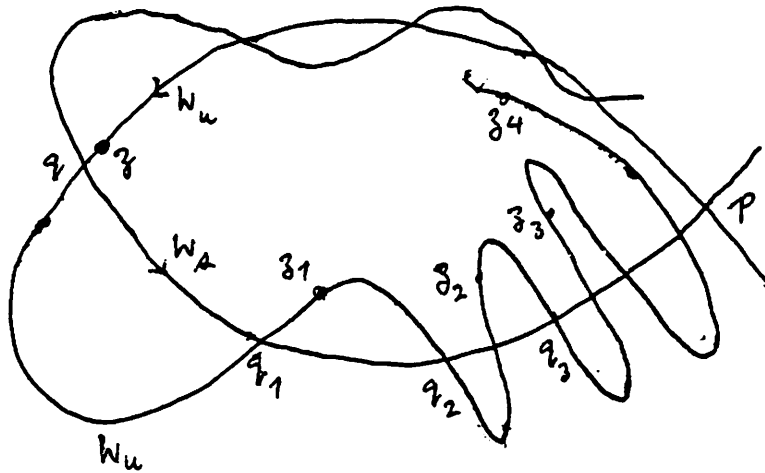


Figure 23: First correction

Correction 2. Now consider a point z on W_u near q as shown in Figure 22. Since $z \in W_u$, its positive iterates will remain on W_u . On the other hand since z is close to q , its positive iterates z_1, z_2, \dots will remain close to q_1, q_2, \dots , respectively, until they approach p . But z_n cannot converge to p since $z \notin W_s$; rather, as z_n comes near p it will swing away in the direction of the unstable manifold W_u . Thus W_u must be modified as in Figure 23.

Correction 3. The same correction must be applied to W_s , since it is the unstable manifold of the system in reverse time. Thus we arrive at the *homoclinic tangle* of Figure 24.

We summarize some of the properties of the homoclinic tangle. Let Λ be the set of points homoclinic to p . Λ is invariant under F , i.e. if x is in Λ then the orbit of x is also in Λ . The proof of the following theorem can be found in [9].

Theorem The dynamics of $F(\cdot; \gamma)$ on Λ is chaotic.

The term chaos is associated with the following properties.

1. *Sensitivity to initial conditions.* For any $q \in \Lambda$ and $\epsilon > 0$, there exists $z \in \Lambda$, with $|z - q| < \epsilon$, such that

$$|F^n(z; \gamma) - F^n(q; \gamma)| > K n^\sigma$$

for some $\sigma > 0$. Thus trajectories starting at arbitrarily close initial points will eventually diverge, making prediction impossible. To see this consider a small rectangular region of initial states around q with sides parallel to W_u and W_s , as in Figure 24. As we iterate this set of states forward in time, the sides parallel to W_u get stretched, the sides parallel to W_s shrink, and the rectangle folds upon itself as the iterates approach the equilibrium p . The stretching action accounts for the insensitivity to initial conditions. The stretching and folding actions make F topologically equivalent to Smale's

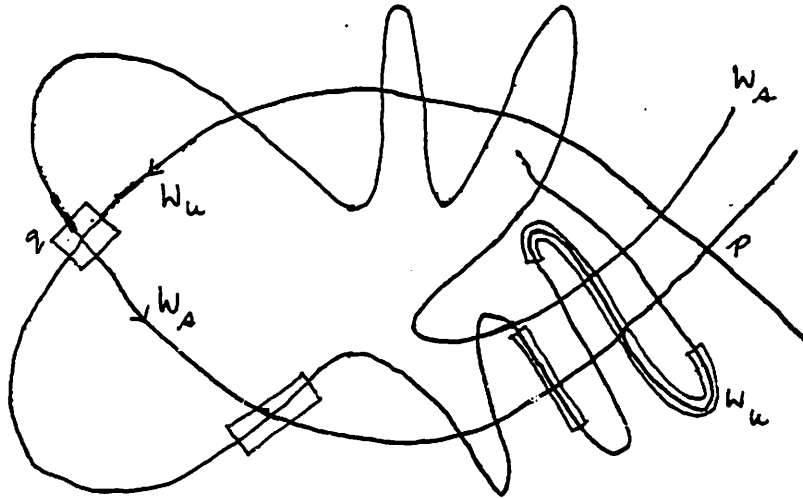


Figure 24: Homoclinic tangle

horseshoe map, [5, 9]. The remaining properties are then deduced from the horseshoe map.

2. *Periodic orbits.* Λ contains periodic orbits of all periods. It also contains infinitely many non-periodic orbits.
3. *Dense orbit.* There is an orbit which is dense in Λ .
4. *Cantor set.* Λ is a Cantor set.

The last property also implies that Λ is a *fractal*, i.e. a subset of the state space (R^2 in our case) of fractional dimension.³³

Having understood the orbit structure of F on Λ we can get a glimpse of the orbit structure of the suspended system (34). The thing to remember is that trajectories of (39) are samples of those of (34) spaced T apart. This is done in Figure 25. The figure is simplified since the orbit structure of F is taken to be like that of Figure 22 rather than the more accurate Figure 24. Figure 25 displays two trajectories, one starts at q_0 , the second starts at p . The samples of the trajectory through q_0 are q_1, q_2, \dots . In the suspended system there is a continuous trajectory $q(t)$ as shown with $q(\delta_0) = q_0, q(\delta_0 + T) = q_2, \dots$. The two planes at $t = \delta_0$ and at $t = \delta_0 + T$ are identified so q_i in the two planes is the same point. The trajectory $p(t)$ through p is periodic, $p(\delta_0) = p(\delta_0 + T) = p$.

³³One definition of dimension of $A \subset R^2$ is this: For each $\epsilon > 0$ cover A by squares of side ϵ as few in number as possible. Suppose this number is $N(\epsilon)$. Then the dimension of A is d if $N(\epsilon) \sim K\epsilon^{-d}$ as $\epsilon \rightarrow 0$. Check that if A is a line segment its dimension is 1, if it is a square its dimension is 2. For the Cantor set Λ , $1 < \text{dimension}(\Lambda) < 2$.

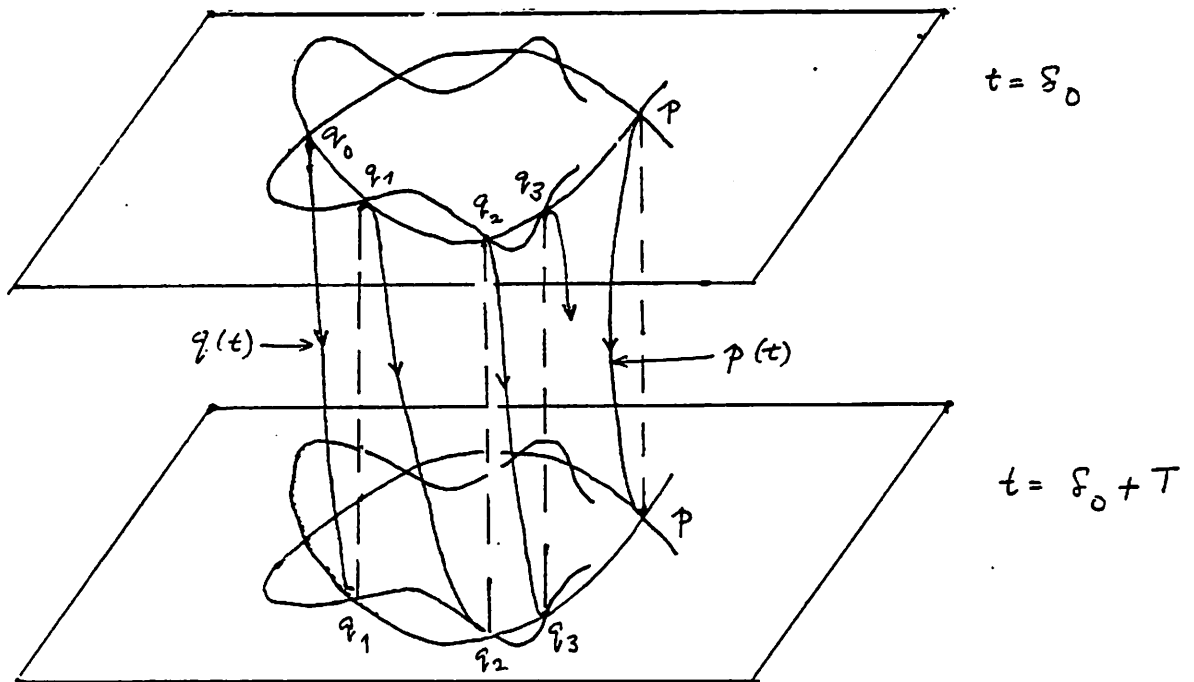


Figure 25: Trajectories of (34)

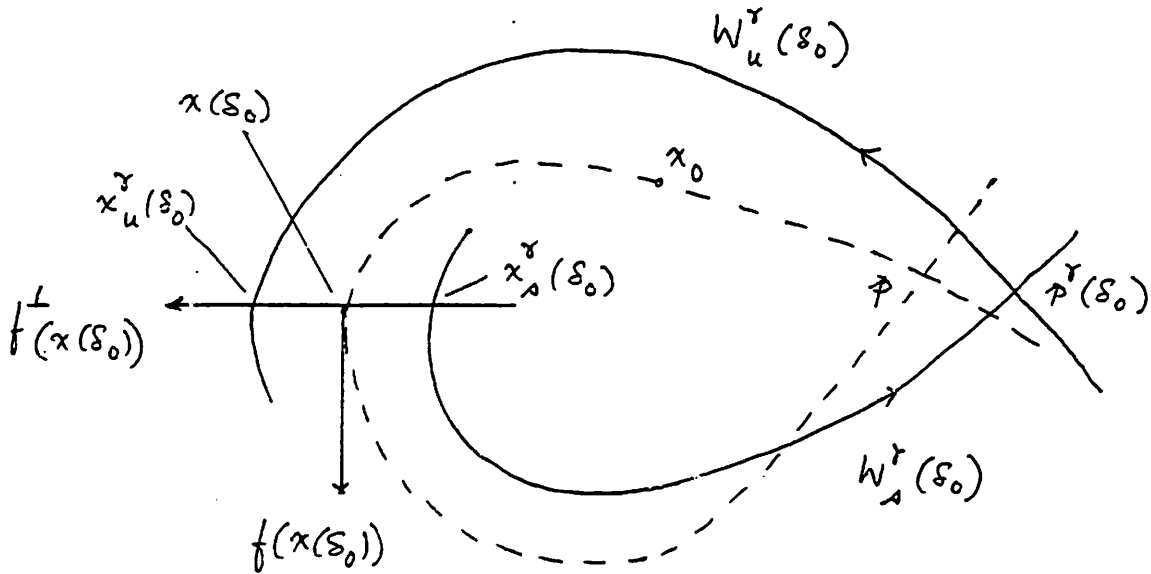


Figure 26: The Melnikov integral

4.1.3 The Melnikov integral

We saw above that if the periodic forcing term breaks up a homoclinic orbit in such a way as to lead to a transversal intersection, then there is a global bifurcation into chaos. In this section we review a technique for determining if a transversal intersection does occur. The material below is adapted from [2, 75].

Consider the perturbed system

$$\dot{x} = f(x) + \gamma g(x, t)$$

Figure 26 displays the orbit structure of the Poincaré map (39). It is drawn as if the result of the breakup of the homoclinic orbit is as in Figure 21 a. The homoclinic orbit itself is depicted by the dashed curve. Fix a point x_0 on this orbit and let $x(t)$, $t \in \mathbb{R}$, be the trajectory of the unperturbed system through x_0 . Fix δ_0 and focus attention on the point $x(\delta_0)$. Note that as δ_0 ranges over $(-\infty, \infty)$, $x(\delta_0)$ ranges over the entire homoclinic orbit.

Draw the straight line through $x(\delta_0)$ perpendicular to the homoclinic orbit. This line is perpendicular to $f(x(\delta_0))$ and parallel to

$$f^\perp(x(\delta_0)) := (-f_2(x(\delta_0)), f_1(x(\delta_0)))$$

Let $x_s^\gamma(\delta_0)$ and $x_u^\gamma(\delta_0)$ be the points where the stable and unstable manifolds of $p^\gamma(\delta_0)$ intersect this line. We can see that

$$d(\delta_0) := \frac{f(x(\delta_0)) \wedge (x_u^\gamma(\delta_0) - x_s^\gamma(\delta_0))}{|f(x(\delta_0))|}$$

is a measure of the separation between $W_u^\gamma(\delta_0)$ and $W_s^\gamma(\delta_0)$ at $x(\delta_0)$. In particular, we note that if $d(\delta_0)$ changes sign for some $\delta_0 \in \mathbb{R}$, then the two manifolds must intersect. Here for vectors y and z ,

$$y \wedge z := y_1 z_2 - y_2 z_1$$

Define the *Melnikov integral*

$$M(\delta_0) = \int_{-\infty}^{\infty} f(x(t - \delta_0)) \wedge g(x(t - \delta_0), t) dt \quad (40)$$

Then the following estimate is valid

$$d(\delta_0) = \frac{\gamma M(\delta_0)}{|f(x(\delta_0))|} + O(\gamma^2)$$

from which the following result follows.

Theorem If $M(\delta_0)$ has simple zeros, then, for $\gamma > 0$ sufficiently small, the manifolds $W_s^\gamma(\delta_0)$ and $W_u^\gamma(\delta_0)$ intersect transversally. If $M(\delta_0) \neq 0$ for all δ_0 then the two manifolds are disjoint.

This provides a test to determine transversal intersection, hence the occurrence of chaos. We will see how this is used to predict chaos in power systems. Note that calculation of the integral (40) will require an explicit (or computable) form for the unperturbed homoclinic orbit $x(t)$ as well as the periodic forcing function $g(x(t - \delta_0), t)$.

4.2 Chaos in power systems

All of the papers dealing with chaos in power systems fall into a pattern. A system of two or more generators is considered. The coupling coefficients (transmission line susceptances) are indexed by a single parameter γ . When $\gamma = 0$, the generators are decoupled. In this decoupled configuration, all except one generator exhibits periodic orbits, while the exceptional generator exhibits a homoclinic orbit. When $\gamma \neq 0$, γ small, the periodic orbits exert a periodic force on the exceptional machine thereby breaking up its homoclinic orbit. The results of §4.1.2 and §4.1.3 are used to show a transversal intersection.

4.2.1 Chaos in a single machine I

We begin with a review of the first paper demonstrating chaos in power systems [76]. The swing equation of a single generator connected to an infinite bus and without damping is

$$\begin{aligned} \dot{\theta} &= \omega \\ M\dot{\omega} &= P - B \sin \theta \end{aligned} \quad (41)$$

Assume $P < B$. Then, as noted in §2.2, there are two equilibria at θ and $\phi = \pi - \theta$ where

$$\theta = \sin^{-1} \frac{P}{B}$$

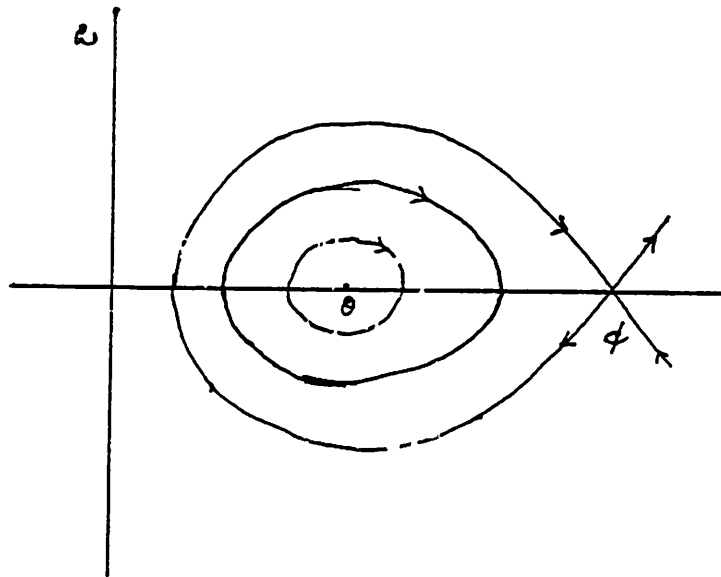


Figure 27: Phase portrait of (41)

ϕ is a saddle. Since there is no damping, θ is no longer a stable node; it is a center. The phase portrait of (41) is shown in Figure 27. It consists of limit cycles surrounding the center ($\omega = 0, \theta$) and filling out the region inside the homoclinic orbit through the saddle.

The trick now is to perturb (41) by a small periodic forcing term. Suppose that our generator is also connected by a small capacity transmission line to another generator. The dynamics of the first generator are then changed from (41) to

$$\begin{aligned} \dot{\theta} &= \omega \\ M\dot{\omega} &= P - B \sin \theta - \gamma f(\theta, t) \end{aligned} \quad (42)$$

where

$$f(\theta, t) = \sin(\theta - \psi(t))$$

and $\psi(t)$ is the voltage angle of the second or 'forcing' generator.

We want to make $\psi(t)$ periodic. Suppose this second generator, which also has no damping, has a very large inertia (compared to M). Then the fact that it is coupled to the first generator will not change its phase portrait significantly. And so its phase portrait will be similar to that of Figure 27. In particular, if the initial conditions of this second generator are properly chosen, it will oscillate in a periodic orbit around its center equilibrium i.e. $\psi(t)$ will be a periodic function. We can now evaluate the Melnikov integral (40) to determine whether the homoclinic orbit is broken up by the periodic forcing term into a transversal intersection. That program is carried out in [76] and it is indeed shown that a transversal intersection can occur. It follows from the Theorem in §4.1.2 that the

first generator exhibits chaotic behavior. The computation of the Melnikov integral involves some complex calculations which will not be reproduced here.

We note, however, that in order to facilitate the analysis some unrealistic parameter choices were made in [76] such as the assumption that the second generator is ‘infinitely’ larger than the first. But it appears that systems involving more realistic parameter values could be analyzed numerically.

4.2.2 A numerical study

A partial attempt along these lines is reported in [77] which considers basically the same system, but there is damping in both generators. The dynamics of the first generator is now given by

$$\begin{aligned}\dot{\theta} &= \omega \\ M\dot{\omega} + D\omega &= P - B \sin \theta - \gamma e^{-\alpha t} f(\theta, t)\end{aligned}\tag{43}$$

In (43) $f(\theta, t)$ is periodic and the damped exponential term reflects the damping of the second generator. One can no longer expect transversal intersection of the stable and unstable manifolds for two reasons. First, the unperturbed system does not have a homoclinic orbit because of the damping term as can be seen in the phase portraits of §2.2. Second, the presence of the damped exponential means that the forcing term is not periodic. One expects at most that the boundary of the stable equilibrium will have a ‘tangled’ shape. Somewhat crude numerical calculations are carried out to show that this is indeed the case.

4.2.3 Chaos in a single machine, II

An interesting demonstration of chaotic behavior is given in [78]. The study deals with two generators whose dynamics are given by (4) for $n = 2$, so we have

$$\begin{aligned}\dot{\theta}_1 &= \omega_1 \\ M_1\dot{\omega}_1 + D_1\omega_1 &= P_1 - B_{13} \sin \theta_1 - \gamma \sin(\theta_1 - \theta_2)\end{aligned}\tag{44}$$

$$\begin{aligned}\dot{\theta}_2 &= \omega_2 \\ M_2\dot{\omega}_2 + D_2\omega_2 &= P_2 - B_{23} \sin \theta_2 - \gamma \sin(\theta_2 - \theta_1)\end{aligned}\tag{45}$$

Bus 3 is the infinite bus. The parameter γ is small; it represents the transmission capacity connecting generator 1 and 2.

Consider the unperturbed system, $\gamma = 0$. The two generators are now uncoupled. We want to arrange initial conditions and the choice of the P_i so that the first generator has a homoclinic orbit (or a heteroclinic cycle) and the second generator has a periodic solution. We can do this readily using the analysis of §2.2. Refer to the bifurcation diagram of Figure 2. In terms of the notation developed there, choose P_1 so that the first generator is on the curve α_0 of Figure 2. The phase portrait is given in Figure 4 and shows a homoclinic orbit

(the saddle connection).³⁴ Choose P_2 for the second generator so that it is in the region EO of Figure 2. The corresponding phase portrait is given by Figure 5. It shows the presence of an orbit marked C which is a stable limit cycle, hence a periodic orbit.

Thus when $\gamma = 0$, the two machines are decoupled, the first machine possesses a homoclinic orbit, and the second possesses a periodic orbit.³⁵ When $\gamma \neq 0$, the second machine will cause a breakup of the homoclinic orbit. For γ small, the Melnikov integral provides a technique for determining transversal intersection. However, since explicit forms for the periodic and homoclinic orbits are not available, this approach is not pursued. Instead, numerical data is presented to show that for different values of damping constants and power inputs both transversal intersections and non-intersections of the stable and unstable manifolds can occur.

Two comments on this study deserve mention. First, although [76] and [78] follow the general pattern mentioned above of discovering bifurcation to chaos, the actual mechanisms are different. Second, the periodic forcing function used in [78], namely the periodic limit cycle C of Figure 5, appears to be unrealistic. This becomes clear upon noting that in following the cycle C , the second generator is no longer in synchronism with the infinite bus – a situation which protection mechanisms would not allow to persist in practice.

4.2.4 Arnold diffusion

In [79] the study of [76] is extended to a system of n generators, see also [80, 81]. Thus the model is that of (4), except that there is no damping ($D_i = 0$, all i). There is no infinite bus, so the sum in (5) only extends up to n . Taking ω_R as a nominal reference frequency, these equations can be expressed as,

$$\begin{aligned}\dot{\theta}_i &= \omega_i - \omega_R \\ M_i \dot{\omega}_i &= P_i - \sum_{j=1}^n B_{ij} \sin(\theta_i - \theta_j), \quad i = 1, \dots, n\end{aligned}\tag{46}$$

This system possesses the Hamiltonian or energy function

$$W = \frac{1}{2} \sum_{i=1}^n M_i (\omega_i - \omega_R)^2 - \sum_{i=1}^n P_i \theta_i - \sum_{i < j} B_{ij} \cos(\theta_i - \theta_j)$$

The energy remains constant along every trajectory of (46).

The B_{ij} are chosen so that machines i and j are coupled weakly unless $j = n$, i.e.

$$B_{ij} = \gamma \beta_{ij}, \quad 1 \leq i, j \leq n - 1$$

When $\gamma = 0$, all machines are coupled only to machine n . In this condition the phase portrait is given by the n -fold ‘product’ of Figure 27. In particular, the first $n - 1$ machines

³⁴In Figure 4 we identify ϕ and $2\pi - \phi$.

³⁵Note that the homoclinic and periodic orbits in this case are both different from those considered in [76].

can have a limit cycle, and the n th machine is on its hyperbolic orbit. This is an approximate picture: actually, since the machines are coupled,

$$\theta \in \Sigma^n := [0, 2\pi]^n$$

(with 0 and 2π identified), the phase portrait is in $R^n \times \Sigma^n$.

The $n - 1$ machines provide a forcing input to the n th machine, resulting in a breakup of the hyperbolic orbit. The situation cannot be analyzed as in [76] since the Melnikov integral (40) only works for planar systems. A vector version of the Melnikov integral is used [82, 83]. The analysis is rather complicated and will not be reproduced. It is shown that chaos can indeed occur for appropriate choice of parameters. In this high dimensional system, the structure of chaotic behavior is quite complex. Recall that the state space is partitioned into constant energy surfaces ($W = \text{constant}$), and a trajectory cannot cross these surfaces. However, whereas in two dimensional systems each constant energy surface ‘confines’ a trajectory into a small region of state space (see Figure 27, where each closed orbit is a constant energy surface), this no longer happens in higher order systems, and a trajectory can ‘wander’ across the state space. The resulting chaotic process is called *Arnold diffusion* [84].

Since the Melnikov method is only valid for small values of γ , this study suffers from the same defect as [76] in that only unrealistic parameter values seem amenable to analytic treatment.

4.3 An appraisal of chaos in power systems

In §2.4.2 we reviewed a fairly general multi-machine model with PQ load buses. Such a model admits a Lyapunov function W . If the generators have positive damping, then W is strictly decreasing along any trajectory that is not at an equilibrium. This result implies that it is impossible to have a limit cycle in a state space where the voltage angles are measured over $(-\infty, \infty)$ instead of modulo 2π . The chaos results of [76, 80] imply precisely such a limit cycle, so those kinds of chaotic behavior *cannot* occur in the presence of damping. Nevertheless, if the damping is sufficiently small, the boundary of the stability will display some features of the ‘homoclinic tangle’, as the numerical study of [77] suggests. We have very little knowledge as to how much this tangled boundary reduces the stability region.

On the other hand, the presence of damping does not preclude the chaotic behavior discovered in [78]. But as we mentioned in discussing that study, the particular limit cycle used there will most likely not be observed in practice.

The Melnikov integral technique used in several studies reveals chaos in systems with unreasonable parameter values, so it is difficult to draw any implications for practice. It does suggest, however, that further progress will require careful numerical studies.

References

- [1] E. N. Lorenz, "Deterministic non-periodic flow," *Journal of the Atmospheric Sciences*, vol. 20, pp. 130–141, 1963.
- [2] J. Guckenheimer and P. Holmes, *Nonlinear Oscillations, Dynamical Systems, and Bifurcations of Vector Fields*. Applied mathematical sciences, vol. 42, Springer, 1986. Second printing.
- [3] J. Gleick, *Chaos: Making a new science*. Viking, 1987.
- [4] I. Ekeland, *Mathematics and the unexpected (Translation)*. University of Chicago Press, 1988.
- [5] G. L. Baker and J. P. Gollub, *Chaotic Dynamics, an introduction*. Cambridge University Press, 1990.
- [6] R. Abraham and C. Shaw, *Dynamics: The Geometry of Behavior, Parts 1-4*. Ariel Press, 1984.
- [7] R. L. Devaney, *An Introduction to Chaotic Dynamical Systems*. Addison-Wesley, 1987.
- [8] E. A. Jackson, *Perspectives of nonlinear dynamics*, vol. 1. Cambridge University Press, 1989.
- [9] S. Wiggins, *Global Bifurcations and Chaos*. Applied mathematical sciences, vol. 73, Springer, 1988.
- [10] A. Arapostathis, S. Sastry, and P. Varaiya, "Global analysis of swing dynamics," *IEEE Transactions on Circuits and Systems*, vol. CAS-29, pp. 673–679, October 1982.
- [11] A. A. Andronov and C. E. Chaikin, *Theory of Oscillations*. Princeton University Press, 1949.
- [12] J. L. Willems, "Direct methods for transient stability studies in power systems analysis," *IEEE Transactions on Automatic Control*, vol. AC-16, pp. 332–341, August 1971.
- [13] C. J. Tavora and O.J.M. Smith, "Stability analysis of power systems," *IEEE Transactions on Power Apparatus and Systems*, vol. PAS-91, pp. 1138–1144, May/June 1972.
- [14] A. Arapostathis, S. Sastry, and P. Varaiya, "Analysis of power-flow equations," *International Journal of Electrical Energy and Power Systems*, vol. 3, pp. 116–126, 1981.
- [15] A. Arapostathis and P. Varaiya, "Behavior of three-node power networks," *International Journal of Electrical Energy and Power Systems*, vol. 5, pp. 22–30, 1983.
- [16] J. Baillieul and C. I. Byrnes, "The load flow equations for a 3-node electric power system," *Systems and Control Letters*, vol. 2, pp. 321–329, April 1983.

- [17] J. Baillieul and C. I. Byrnes, "The singularity theory of the load flow equations for a 3-node electric power system," *Systems and Control Letters*, vol. 2, pp. 330–340, April 1983.
- [18] A. J. Korsak, "On the question of uniqueness of stable load flow solutions," *IEEE Transactions on Power Apparatus and Systems*, vol. PAS-91, pp. 1093–1100, 1972.
- [19] J. Baillieul and C. I. Byrnes, "Geometric critical point analysis of lossless power system models," *IEEE Transactions on Circuits and Systems*, vol. CAS-29, pp. 724–737, November 1982.
- [20] R. Gilmore, *Catastrophe Theory for Scientists and Engineers*. New York: Wiley, 1981.
- [21] J. Milnor, *Morse Theory*. Princeton University Press, 1963.
- [22] R. Thom, *Stability and Morphogenesis (Translation)*. Benjamin, 1975.
- [23] A. A. Sallam and J. L. Dineley, "Catastrophe theory as a tool for determining synchronous power system dynamic stability," *IEEE Transactions on Power Apparatus and Systems*, vol. PAS-102, pp. 622–630, March 1983.
- [24] J. L. Dinneley and G. A. Mahmoud, "A new method of on-line evaluation of synchronous power system stability," in *IEE 2nd International Conference on Power Monitoring and Control*, pp. 333–338, 1986.
- [25] M. D. Wvong and A. M. Mihirig, "Catastrophe theory applied to transient stability assessment of power systems," *IEE Proceedings, Part C*, vol. 133, pp. 314–318, September 1986.
- [26] A. M. Mihirig and M. D. Wvong, "Application of catastrophe theory to transient stability analysis of power systems," in *IASTED International Conference on Power High Technology*, pp. 101–105, 1986.
- [27] A. A. Sallam, "Power systems steady state stability assessment using catastrophe theory," *IEE Proceedings, Part C*, vol. 135, pp. 189–194, May 1988.
- [28] A. A. Sallam, "Power systems transient stability assessment using catastrophe theory," *IEE Proceedings, Part C*, vol. 136, pp. 108–114, March 1989.
- [29] A. M. Mihirig and M. D. Wvong, "Transient stability analysis of multimachine power systems by catastrophe theory," *IEE Proceedings, Part C*, vol. 136, pp. 254–258, July 1989.
- [30] N. Narasimhamurthi, "On the existence of energy function for power systems with transmission losses," *IEEE Transactions on Circuits and Systems*, vol. CAS-31, pp. 199–203, February 1984.
- [31] H. G. Kwatny, L. Y. Bahar, and A. K. Pasrija, "Energy-like lyapunov functions for power system stability analysis," *IEEE Transactions on Circuits and Systems*, vol. CAS-32, pp. 1140–1149, November 1985.

- [32] H.-D. Chiang, "Study of the existence of energy functions for power systems with losses," *IEEE Transactions on Circuits and Systems*, vol. CAS-36, pp. 1423–1429, November 1989.
- [33] H.-D. Chiang, F. F. Wu, and P. Varaiya, "Foundations of the potential energy boundary surface method for power system transient stability analysis," *IEEE Transactions on Circuits and Systems*, vol. CAS-36, pp. 712–728, June 1988.
- [34] M. A. Pai, *Power System Stability*. North-Holland, 1981.
- [35] J. K. Hale, "Generic bifurcation with applications," in *Nonlinear analysis and mechanics: Heriot Watt Symposium*, pp. 59–156, 1977.
- [36] E. H. Abed and P. Varaiya, "Oscillations in power systems via Hopf bifurcation," in *Proceedings of the 27th IEEE Conference on Decision and Control*, (San Diego), pp. 926–929, December 1981.
- [37] P. M. Anderson and A. A. Fouad, *Power System Control and Stability*, vol. 1. The Iowa State University Press, 1977.
- [38] N. Tsolas, A. Arapostathis, and P. Varaiya, "A structure preserving energy function for power system transient stability analysis," *IEEE Transactions on Circuits and Systems*, vol. CAS-32, pp. 1041–1049, October 1985.
- [39] A. R. Bergen and D. J. Hill, "A structure preserving model for power system stability analysis," *IEEE Transactions on Power Apparatus and Systems*, vol. PAS-100, pp. 25–35, 1981.
- [40] N. Narasimhamurthi and M. R. Musavi, "A generalized energy function for transient stability analysis of power systems," *IEEE Transactions on Circuits and Systems*, vol. CAS-31, pp. 637–645, July 1984.
- [41] H. G. Kwatny, A. K. Pasrija, and L. Y. Bahar, "Static bifurcations in electric power networks: Loss of steady-state stability and voltage collapse," *IEEE Transactions on Circuits and Systems*, vol. CAS-33, pp. 981–991, October 1986.
- [42] S. S. Sastry and C. A. Desoer, "Jump behavior of circuits and systems," *IEEE Transactions on Circuits and Systems*, vol. CAS-28, pp. 1109–1124, December 1981.
- [43] V. A. Venikov, V. A. Stroeve, V. I. Idelchick, and V. I. Tarasov, "Estimation of electric power systems steady-state stability in load flow calculations," *IEEE Transactions on Power Apparatus and Systems*, vol. PAS-94, pp. 1934–1938, May/June 1975.
- [44] S. Abe, N. Hamada, A. Isono, and K. Okuda, "Load flow convergence in the vicinity of a voltage instability," *IEEE Transactions on Power Apparatus and Systems*, vol. PAS-97, pp. 1983–1993, November/December 1978.
- [45] Y. Tamura, H. Mori, and S. Iwamoto, "Relationship between voltage stability and multiple load flow solutions in electric power systems," *IEEE Transactions on Power Apparatus and Systems*, vol. PAS-102, pp. 1115–1125, May 1983.

- [46] A. Yokoyama and Y. Sekine, "A static voltage stability index based on multiple load flow solutions," in *Proceedings: Bulk Power System Voltage Phenomena - Voltage Stability and Security*, pp. 7-111 - 7-123, EPRI Report EL-6183, 1989.
- [47] J. E. Koehler, "'henniker revisited' Meeting the challenges of today and tomorrow through communication and research," in *Proceedings: Bulk Power System Voltage Phenomena - Voltage Stability and Security*, pp. 1-1 - 1-4, EPRI Report EL-6183, 1989.
- [48] Y. Sekine, A. Yokoyama, and T. Kumano, "A method for detecting a critical state of voltage collapse," in *Proceedings: Bulk Power System Voltage Phenomena - Voltage Stability and Security*, pp. 5-65 - 5-72, EPRI Report EL-6183, 1989.
- [49] R. A. Schleuter, A. G. Costi, J. E. Sekerke, and H. L. Forge, "Voltage stability and security assessment," tech. rep., EPRI Draft Final Report, PR-1999-8, February 1987.
- [50] R. Navarro-Perez, B. J. Cory, and M. Short, "Voltage collapse proximity analysis using reactive area identification," in *Proceedings: Bulk Power System Voltage Phenomena - Voltage Stability and Security*, pp. 7-41 - 7-58, EPRI Report EL-6183, 1989.
- [51] Y. Tamura, "Voltage instability proximity index based on multiple load-flow solutions in ill-conditioned power systems," in *Proceedings of the 27th IEEE Conference on Decision and Control*, (Austin, TX.), pp. 2114-2119, December 1988.
- [52] C. C. Liu and K. T. Vu, "A summary of results on voltage stability analysis," in *Proceedings: Bulk Power System Voltage Phenomena - Voltage Stability and Security*, pp. 6-81 - 6-87, EPRI Report EL-6183, 1989.
- [53] Y. Tamura, T. Ogata, T. Motoyoshi, Y. Tayama, and Y. Nakanishi, "Interactions between regulating equipments in voltage instability environment," in *Proceedings of the 28th IEEE Conference on Decision and Control*, (Tampa, FL.), pp. 326-331, December 1989.
- [54] C. L. DeMarco and A. R. Bergen, "A security measure for random load disturbances in nonlinear power system models," *IEEE Transactions on Circuits and Systems*, vol. CAS-34, pp. 1546-1557, December 1987.
- [55] P. Varaiya, F. F. Wu, and R.-L. Chen, "Direct methods for transient stability of power systems: recent results," *Proceedings of the IEEE*, vol. 73, pp. 1703-1715, December 1985.
- [56] I. Dobson and H. D. Chiang, "Towards a theory of voltage collapse in electric power systems," *System and Control Letters*, vol. 13, pp. 253-262, September 1989.
- [57] H. D. Chiang, M. Hirsch, and F. F. Wu, "Stability regions of nonlinear autonomous dynamical systems," *IEEE Transactions on Automatic Control*, vol. AC-33, pp. 14-27, January 1988.

- [58] H. D. Chiang, I. Dobson, R. J. Thomas, J. S. Thorp, and F. A. Lazhar, "On the voltage collapse in power systems," *IEEE Transactions on Power Systems*, vol. 5, pp. 601–611, May 1990.
- [59] J. Marsden and M. McCracken, *The Hopf Bifurcation and its Applications*. Applied mathematical sciences, vol. 19, Springer, 1976.
- [60] A. I. Mees and L. O. Chua, "The Hopf bifurcation theorem and its application to nonlinear oscillations in circuits and systems," *IEEE Transactions on Circuits and Systems*, vol. CAS-26, pp. 235–254, April 1979.
- [61] B. D. Hassard, N. D. Kazarinoff, and Y.-H. Wan, *Theory and Applications of Hopf Bifurcation*. London Mathematical Society Lecture Notes Series, 41, Cambridge University Press, 1981.
- [62] E. H. Abed and P. Varaiya, "Nonlinear oscillations in power systems," *International Journal of Electric Power and Energy Systems*, vol. 6, pp. 37–43, January 1984.
- [63] J. Hale, *Ordinary Differential Equations*. Robert E. Krieger Publishing Company, 1980.
- [64] F. P. deMello and C. Concordia, "Concepts of synchronous machine stability as affected by excitation control," *IEEE Transactions on Power Apparatus and Systems*, vol. PAS-88, pp. 316–329, 1969.
- [65] R. T. Byerley and E. W. K. Eds, *Stability of Large Electric Power Systems*. IEEE Press, 1974.
- [66] J. E. Van Ness, F. M. Brasch Jr., G. L. Landgren, and S. I. Neumann, "Analytical investigation of dynamic instability occurring at powerton station," *IEEE Transactions on Power Apparatus and Systems*, vol. PAS-99, pp. 1386–1395, July/August 1980.
- [67] E. H. Abed, N. Tsolas, and P. Varaiya, "Study of nonlinear oscillations due to exciter control," in *Proceedings 1983 IEEE International Symposium on Circuits and Systems*, (Newport Beach, CA), pp. 1410–1413, May 1983.
- [68] C. Rajagopalan, P. W. Sauer, and M. A. Pai, "Analysis of voltage control systems exhibiting Hopf bifurcation," in *Proceedings of the 28 IEEE Conference on Decision and Control*, (Tampa, FL), pp. 332–335, December 1989.
- [69] E. H. Abed, "Singularly perturbed Hopf bifurcation," *IEEE Transactions on Circuits and Systems*, vol. CAS-32, pp. 1270–1280, December 1985.
- [70] M. Golubitsky and W. F. Langford, "Classification and unfoldings of degenerate Hopf bifurcation," *Journal of Differential Equations*, vol. 41, no. 3, pp. 375–415, 1981.
- [71] R.-L. Chen and P. Varaiya, "Degenerate Hopf bifurcation in power systems," *IEEE Transactions on Circuits and Systems*, vol. CAS-35, pp. 818–824, July 1988.
- [72] M. Golubitsky and D. G. Schaeffer, *Singularities and Groups in Bifurcation Theory*, vol. I. Springer, 1985.

- [73] M. M. Liwshitz, "Positive and negative damping in synchronous machines," *AIEE Transactions*, vol. 60, pp. 210–213, May 1941.
- [74] C. Concordia and G. K. Carter, "Negative damping of electrical machinery," *AIEE Transactions*, vol. 60, pp. 116–119, March 1941. Discussion p. 752.
- [75] F.M.A. Salam, "The Mel'nikov technique for highly dissipative systems," *SIAM Journal of Applied Mathematics*, vol. 47, pp. 232–243, April 1987.
- [76] N. Kopell and R. B. Washburn Jr., "Chaotic motions in the two-degree-of-freedom swing equations," *IEEE Transactions on Circuits and Systems*, vol. CAS-29, pp. 738–746, November 1982.
- [77] M. Varghese and J. S. Thorp, "An analysis of truncated fractal growths in the stability boundaries of three-node swing equations," *IEEE Transactions on Circuits and Systems*, vol. CAS-35, pp. 825–834, July 1988.
- [78] F.M.A. Salam, S. Bai, and S. Guo, "Chaotic dynamics even in the highly damped swing equations of power systems," in *Proceedings of the 27th IEEE Conference on Decision and Control*, (Austin, TX.), p. ????, December 1988.
- [79] F.M.A. Salam, J. Marsden, and P. Varaiya, "Arnold diffusion in swing equations of a power system," *IEEE Transactions on Circuits and Systems*, vol. CAS-30, pp. 673–688, August 1984.
- [80] F.M.A. Salam, J. E. Marsden, and P. P. Varaiya, "Chaos and Arnold diffusion in dynamical systems," *IEEE Transactions on Circuits and Systems*, vol. CAS-30, pp. 697–708, September 1983.
- [81] F.M.A. Salam, J. E. Marsden, and P. P. Varaiya, "Arnold diffusion in the dynamics of a 4-machine power system undergoing a large fault," in *Proceedings of the 22nd IEEE Conference on Decision and Control*, (San Antonio, TX.), pp. 1411–1414, December 1983.
- [82] P. Holmes, "Averaging and chaotic motions in forced oscillations," *SIAM Journal on Applied Mathematics*, vol. 38, pp. 65–80, 1978.
- [83] P. Holmes, "Averaging and chaotic motions in forced oscillations: Errata and Addenda," *SIAM Journal on Applied Mathematics*, vol. 40, pp. 167–168, 1980.
- [84] P. Holmes and J. E. Marsden, "Melnikov's method and Arnold diffusion for perturbations of integrable Hamiltonian systems," *Journal of Mathematical Physics*, vol. 23, no. 4, pp. 669–679, 1982.